



Cooper, F. J., Hodges, K. V., & Adams, B. A. (2013). Metamorphic constraints on the character and displacement of the South Tibetan fault system, central Bhutanese Himalaya. *Lithosphere*, 5(1), 67-81. DOI: 10.1130/L221.1

Peer reviewed version

Link to published version (if available):  
[10.1130/L221.1](https://doi.org/10.1130/L221.1)

[Link to publication record in Explore Bristol Research](#)  
PDF-document

This is the author accepted manuscript (AAM). The final published version (version of record) is available online via GSA at <http://lithosphere.gsapubs.org/content/5/1/67>. Please refer to any applicable terms of use of the publisher.

## **University of Bristol - Explore Bristol Research**

### **General rights**

This document is made available in accordance with publisher policies. Please cite only the published version using the reference above. Full terms of use are available:  
<http://www.bristol.ac.uk/pure/about/ebr-terms.html>

1 Metamorphic constraints on the character and displacement of  
2 the South Tibetan fault system, central Bhutanese Himalaya

3 F.J. Cooper<sup>1</sup>, K.V. Hodges<sup>1</sup>, and B.A. Adams<sup>1</sup>

4 <sup>1</sup>*School of Earth and Space Exploration, Arizona State University, Tempe, Arizona 85287, USA*

5

6 **ABSTRACT**

7 The South Tibetan fault system (STFS), a family of primarily extensional faults that separates  
8 the metamorphic core of the Himalaya (expressed as the Greater Himalayan sequence (GHS))  
9 from overlying, predominately unmetamorphosed Tibetan sedimentary sequence (TSS) units, has  
10 been mapped for over 2,000 km coincident with the Himalayan range crest. In most areas, the  
11 immediate hanging wall of the STFS sole detachment consists of predominately carbonate rocks  
12 of lower Paleozoic age. However, in the Bhutan sector of the eastern Himalaya (ca. 89–92°E),  
13 the hanging wall of the sole structure is instead frequently mapped at the base of a  
14 metamorphosed, predominately siliciclastic succession (the Chekha Formation), and the base of  
15 the overlying predominately carbonate rocks (Pele La and Tang Chu Groups) is mapped as a less  
16 significant splay of the STFS. Unfortunately, poor exposures throughout central Bhutan make  
17 mapping and structural interpretation of these important contacts difficult, resulting in many  
18 disparities among geologic maps made by different research groups. The STFS in other parts of  
19 the Himalaya accommodates a significant metamorphic discontinuity that should also be  
20 apparent in Bhutan. Therefore, as an alternative approach, we have used the Raman spectroscopy  
21 on carbonaceous material (RSCM) thermometer to evaluate the evidence for a metamorphic  
22 discontinuity across both putative STFS structures.

23 RSCM thermometric data from 17 samples across three purported STFS klippen in central  
24 Bhutan (the Dang Chu, Ura, and Zhemgang klippen) suggest that the contact between the  
25 Chekha Formation and the underlying GHS is not a fault with large, postmetamorphic  
26 displacement. We find no resolvable change in peak metamorphic temperature across the  
27 contact, with a consistent temperature of ca. 560°C, but we see a 130–140°C drop in  
28 paleotemperature across the higher contact between the Chekha Formation and overlying Pele La  
29 and Tang Chu groups. This change coincides with a major change in structural style, from high-  
30 strain, leucogranite-bearing rocks below to large-scale recumbently folded marbles above.  
31 Together, the change in deformational character and metamorphic grade suggest that the  
32 principal STFS detachment in Bhutan is the structural boundary of the Chekha Formation and the  
33 predominantly carbonate rocks above. The presence of an STFS detachment approximately 80  
34 km south of the main STFS fault trace at the crest of the Himalaya, with no match between  
35 correlative footwall and hanging wall units along the direction of fault motion implies large  
36 displacements on the STFS in the eastern Himalaya.

37

38 Keywords: Himalaya; extension; Raman spectroscopy of carbonaceous material;  
39 geothermobarometry

## 40 INTRODUCTION

41 Over the past few decades the eastern Himalayan Kingdom of Bhutan has become increasingly  
42 accessible to foreign visitors, resulting in a flurry of geologic research that has added critical new  
43 information to our understanding of the Himalayan-Tibetan orogenic system (Carosi et al., 2006;  
44 Chakungal et al., 2010; Chambers et al., 2011; Cooper et al., in press; Corrie et al., 2012; Daniel  
45 et al., 2003; Davidson et al., 1997; Edwards et al., 1999; Edwards and Harrison, 1997; Gansser,  
46 1983; Grujic et al., 2006; Grujic et al., 2002; Grujic et al., 2011; Hughes et al., 2011; Kellett et  
47 al., 2009; Kellett et al., 2010; Kellett and Grujic, 2012; Long and McQuarrie, 2010; Long et al.,  
48 2011a; Long et al., 2011b; Long et al., 2011c; Stüwe and Foster, 2001; Swapp and Hollister,  
49 1991; Tobgay et al., 2012). However, research progress has been hindered by the dense  
50 vegetation and shortage of roads (and, in turn, road-cut outcrops) throughout most of the country.  
51 Only in the areas near the Tibetan border are outcrops sufficient to tightly constrain geologic  
52 mapping. As a result, there are still many disparities among geologic maps of Bhutan made by  
53 different research groups. One outstanding issue regards the position, character, and  
54 displacement of the principal basal (or “sole”) detachment of the South Tibetan fault system  
55 (STFS), a family of primarily extensional faults that crops out for over 2,000 km along the length  
56 of the Himalayan range crest (Burchfiel et al., 1992; Burg and Chen, 1984; Hodges et al., 1992;  
57 Pognante and Benna, 1993; Searle et al., 1997; Searle, 1999).

58 Basal low-angle detachments of this system typically mark a metamorphic discontinuity  
59 between high-grade metamorphic gneisses and anatexites of the Himalayan core below and  
60 lower-grade or unmetamorphosed strata above (Burchfiel et al., 1992). Recent mapping in the  
61 central Bhutan Himalaya (Figures 1 and 2) suggests that there may be multiple detachments of  
62 the South Tibetan fault system there (e.g. Carosi et al., 2006; Edwards and Harrison, 1997;

63 Grujic et al., 2006; Grujic et al., 2002; Grujic et al., 2011; Kellett et al., 2009; Kellett et al., 2010;  
64 Kellett and Grujic, 2012; Long and McQuarrie, 2010; Long et al., 2011a; Long et al., 2011c), an  
65 observation similar to that made in several other parts of the orogen where structurally higher  
66 detachments are typically marked by tectonite fabrics but not by significant metamorphic  
67 discontinuities (Burchfiel et al., 1992; Hodges et al., 1994; Hodges et al., 1996; Searle and  
68 Godin, 2003; Searle, 1999).

69 The role of the extensional STFS in the development of the Himalayan orogen is a matter of  
70 active debate, largely because constraining the magnitude of its displacement has proved  
71 difficult. Generally exposed along the Himalayan range crest, down-dip exposures of STFS  
72 detachments that allow direct measurements of minimum displacement are rare. In a recent study  
73 in NW Bhutan, Cooper et al. (in press) traced the STFS from the range crest south for ca. 65 km,  
74 suggesting large displacements on the system. The presence of STFS detachments even farther  
75 south in central Bhutan suggests that minimum displacements on the STFS could be even larger.  
76 Grujic et al. (2011), for example, map the STFS ca. 100 km south of the range crest (Figure 2b).  
77 Alternatively, mapping by Long and McQuarrie (2010) implies that the breakaway zone for the  
78 STFS is present in southern Bhutan. The structural offset between this breakaway and hanging  
79 wall units to the north is at most 20 km suggesting limited slip on the STFS.

80 The differences in mapping and interpretation of the STFS in central Bhutan suggests that  
81 further work is needed in order constrain the position and thus the significance of the system  
82 there. Due to the poor exposures in Bhutan, which have hindered mapping of STFS structures  
83 thus far, we have used the widely-applicable Raman spectroscopy on carbonaceous material  
84 (RSCM) thermometer to evaluate the evidence for metamorphic discontinuities across the  
85 putative STFS structures mapped by previous workers.

86

## 87 **STRUCTURAL SETTING**

### 88 **The Himalayan-Tibetan orogenic system**

89 The Himalayan-Tibetan orogenic system is one of our planet's most spectacular signatures of  
90 continent-continent collision. Thought to have initiated in the Early Eocene with the closure of  
91 the neo-Tethys Ocean (de Sigoyer et al., 2000; Guillot et al., 2008; Leech et al., 2005; Rowley,  
92 1996), collision of the Indian and Eurasian plates created both the highest mountain range and  
93 the most expansive area of regional uplift on Earth: the Tibetan Plateau. The Himalayan sector of  
94 the orogenic system comprises four broad lithotectonic belts of contrasting metamorphic grade  
95 separated by a series of north-dipping faults (Gansser, 1964; Heim and Gansser, 1939; Hodges,  
96 2000; Le Fort, 1975). From south to north, these are the Subhimalayan zone, Lesser Himalayan  
97 zone, Greater Himalayan zone, and Tibetan zone. Each of these zones comprises a distinctive  
98 package of rocks known as the Eocene to Lower Miocene Rawalpindi and Lower Miocene to  
99 Pleistocene Siwalik Groups of the Subhimalayan zone, the Proterozoic to Middle(?) Miocene  
100 Lesser Himalayan sequence (LHS), the Neoproterozoic to Ordovician Greater Himalayan  
101 sequence (GHS), and the Paleozoic to Eocene Tibetan sedimentary sequence (TSS) (Acharyya  
102 and Sastry, 1979; Brasier and Singh, 1987; Brookfield, 1993; Burbank et al., 1997; Critelli and  
103 Garzanti, 1994; DeCelles et al., 1998; Gaetani and Garzanti, 1991; Gansser, 1983; Hodges, 2000;  
104 Najman et al., 1993; Najman et al., 1997; Parrish and Hodges, 1996; Singh et al., 1999; Stöcklin,  
105 1980; Valdiya, 1980). Rocks of the Subhimalaya, LHS, and GHS are separated by orogen-  
106 parallel contractional structures of the Main Boundary thrust system (MBTS) and the Main  
107 Central thrust system (MCTS). In the Bhutanese Himalaya, an out-of-sequence thrust fault (the  
108 Kakhtang thrust) mapped by Gansser (1983) has been interpreted to have roughly doubled the

109 thickness of the GHS (Davidson et al., 1997; Grujic et al., 2002) (Figure 1), although the  
110 location, age and displacement across this structure are poorly constrained. In contrast to its  
111 southern and lower boundary, the top of the GHS is bounded by extensional faults and shear  
112 zones of the STFS. The opposing-sense STFS and MCTS are both thought to have been active  
113 during the Miocene (Hodges et al., 1992; Hodges et al., 1996; Hubbard and Harrison, 1989;  
114 Searle and Rex, 1989), implying that the STFS played an important role in exhuming the GHS  
115 metamorphic core.

116 The structurally highest and northernmost zone is represented by the Tibetan sedimentary  
117 sequence (TSS), which generally crops out north of the Himalayan range crest. The TSS  
118 comprises low-grade to unmetamorphosed sediments deposited on the northern passive  
119 continental margin of India (Gaetani and Garzanti, 1991). Although it is generally accepted that  
120 the GHS and the TSS are separated by the STFS throughout most of the Himalaya, the  
121 relationships are more controversial in regions south of the range crest where the TSS occurs in a  
122 series of low-elevation outliers above GHS lithologies. In some cases, these contacts – typically  
123 poorly exposed – have been interpreted as detachments (presumably strands of the STFS),  
124 whereas they have been interpreted as depositional in others (Gehrels et al., 2003; Grujic et al.,  
125 2002; Robinson et al., 2006; Stöcklin, 1980). In Bhutan, both depositional and tectonic  
126 relationships have been reported for these outliers (e.g. Long and McQuarrie, 2010).

127

### 128 **The South Tibetan fault system**

129 The South Tibetan Fault system was first recognized in central Nepal (Caby et al., 1983) and  
130 later described in southern Tibet (Burchfiel et al., 1992; Burg and Chen, 1984) and northwest  
131 India (Herren, 1987; Searle, 1986; Valdiya, 1989). Although it comprises a variety of fault types

132 including steeply dipping transfer faults (Wu et al., 1998) and low-angle, oblique faults with a  
133 significant component of strike slip motion (Pêcher, 1991), most descriptions focus on the basal  
134 structure of the system, a low-angle, north-dipping fault and associated ductile shear zone  
135 commonly referred to as the South Tibetan detachment.

136 The presence of the STFS within a zone of continental collision has led to considerable debate  
137 regarding its initiation and role in the construction of the orogen (e.g. Hodges, 2000; Law et al.,  
138 2006 and references therein). Two principal models have been put forward to explain its  
139 existence. In the first, the STFS forms a collection of passive roof faults over an evolving  
140 contractional orogenic wedge (e.g. Robinson et al., 2006; Yin, 2006; Yin et al., 1994). In this  
141 case, the STFS has only a minor role in extrusion with minimal displacement across the structure  
142 and little excision of material in the footwall. In the second, the MCTS and STFS are  
143 kinematically linked structures that collectively sustained Miocene southward extrusion of the  
144 metamorphic core of the Himalaya (Beaumont et al., 2001; Godin et al., 2006 and references  
145 therein; Grujic et al., 2002; Hodges et al., 2001; Nelson et al., 1996). This concept, often referred  
146 to as the ‘channel flow’ model, implies that the STFS would have accommodated many  
147 kilometers of displacement and is responsible for excision of several kilometers of structural  
148 section within the GHS (Searle et al., 2006).

149 However, because of the geographic coincidence of many of the basal detachments with the  
150 Himalayan range crest and the relatively subdued relief north of the crest, most of these  
151 structures cannot be traced far down dip, and their net displacements are derived from indirect  
152 geothermobarometric measurements (15–200 km: Cottle et al., 2011; Cottle et al., 2007; Dèzes et  
153 al., 1999; Searle et al., 2003; Searle et al., 2002; Walker et al., 1999) and studies of fault-related  
154 telescoped isograds (25–170 km: Herren, 1987; Law et al., 2011). Exceptions occur in the Mount



155 Everest region of Nepal and the Mount Jomolhari region of NW Bhutan, where components of  
156 the STFS can be traced parallel to their slip vectors, with no match between correlative footwall  
157 and hanging wall units for  $\geq 34$  km in Nepal (Carosi et al., 1998; Hodges et al., 1992) and  $\geq 65$   
158 km in Bhutan (Cooper et al., in press), implying minimum displacements comparable to ca. 75–  
159 140 km minimum estimates for broadly contemporaneous S-directed slip on the Main Central  
160 Thrust system (MCTS) in the eastern Himalaya (Yin, 2006; Yin et al., 2010).

161 The STFS footwall comprises high-grade (upper amphibolite facies) paragneisses and  
162 orthogneisses of the GHS with abundant leucogranite sills, dikes, and plutons. Near the top of the  
163 footwall, these rocks are strongly deformed and most exposures contain well-developed S-C  
164 mylonites (Lister and Snoke, 1984) indicative of hanging wall down-to-the north (normal-sense)  
165 shearing with varying degrees of oblique slip. In most mapped transects, the basal detachment  
166 carries unmetamorphosed lower Paleozoic sedimentary rocks of the TSS in its immediate  
167 hanging wall (e.g. Herren, 1987 (India); Hodges et al., 1993 (southern Tibet)). In two areas – the  
168 Annapurna Range of central Nepal (e.g., Brown and Nazarchuk (1993)) and the Everest region  
169 of eastern Nepal (e.g., Searle, 1999) – hanging wall TSS units also experienced greenschist to  
170 lower or middle amphibolite facies metamorphism, but the STFS still marks a significant  
171 discontinuity in metamorphic pressures and temperatures.

172 Studies of the STFS in Tibet (Burchfiel et al., 1992; Hodges et al., 1994) and Nepal (Hodges  
173 et al., 1996; Searle and Godin, 2003; Searle, 1999) show that wherever the basal detachment  
174 carries metamorphosed TSS rocks in its hanging wall, there is at least one major detachment of  
175 the STFS at a structurally higher level. These structures typically place stratigraphically younger  
176 TSS lithologies on older lithologies, or lower grade (or unmetamorphosed) rocks on higher grade  
177 rocks. The character of deformation along and above the STFS detachments depends on the

178 hanging wall lithology. Observations of the STFS in various localities in Nepal suggest that,  
179 when the basal detachment carries lower amphibolite or greenschist facies rocks in its hanging  
180 wall, there is typically a relatively wide shear zone above and below the detachment but often  
181 also a relatively sharp brittle-ductile shear zone at the contact itself (e.g. Deorali detachment:  
182 Hodges et al., 1996; Lhotse detachment: Searle, 1999; Annapurna detachment: Vannay and  
183 Hodges, 1996). Both ductile and brittle fabrics are transposed into parallelism with the  
184 detachment, indicating syn-detachment development. When the hanging wall is  
185 unmetamorphosed or weakly metamorphosed, there is a well-developed, relatively wide shear  
186 zone beneath the detachment and a usually pronounced (but sometimes thin) breccia zone at the  
187 contact. The breccia zone is oriented subparallel to the shear fabric in the footwall but the  
188 hanging wall-footwall contact is marked by an obvious cut-off of hanging wall strata, sometimes  
189 at a very high angle. Leucogranites cut the basal STFS detachment in several well-studied areas  
190 (e.g. Hodges et al., 1996), but examples of them cutting the upper detachment (e.g. Guillot et al.,  
191 1994; Hodges et al., 1998) are extremely rare.

192

### 193 **The South Tibetan fault system in Bhutan and adjacent areas of Tibet**

194 In the first regional study of the STFS, Burchfiel et al. (1992) mapped two transects across the  
195 GHS–TSS boundary just north of Bhutan at Wagye La and Lhozag-La Kang (Figure 1). In the  
196 Wagye La area, the contact is not exposed, but the topography and outcrop pattern indicate that it  
197 must dip shallowly northward, subparallel to well-developed S-C mylonitic planar fabrics in the  
198 footwall. The contact was interpreted by Burchfiel et al. (1992) as a segment of the basal  
199 detachment of the STFS, with classic GHS footwall units including amphibolite facies  
200 orthogneisses and psammitic and pelitic schists, all intruded by leucogranite sills and dikes. The

201 hanging wall units (low-grade Ordovician marbles and phyllites) are themselves cut by a well-  
202 exposed upper detachment that carries unmetamorphosed Carboniferous-Permian limestones in  
203 its hanging wall.

204 At Lhozag La Kang, the principal STFS detachment has been deformed into ca. 10 km-  
205 wavelength, upright folds and subsequently cut by steeply N-dipping, E-striking normal faults  
206 with relatively minor displacement (Burchfiel et al., 1992; Edwards et al., 1999). This  
207 detachment cuts and thus postdates the ca. 12.5 Ma Khula Kangri leucogranite pluton (Edwards  
208 and Harrison, 1997) (Figure 1). At Gonto La (Edwards et al., 1996) (Figure 1), the detachment  
209 also cuts an older, structurally lower STFS detachment that is intruded by the Khula Kangri  
210 pluton.

211 In the central latitudes of Bhutan, Gansser (1983) mapped synformal erosional remnants of  
212 TSS lithologies above GHS units far south of the main outcrop trace of the STFS along the  
213 Bhutan-Tibet border (Figure 1). The structurally and stratigraphically highest units in the  
214 erosional remnants are Precambrian-Devonian(?), locally fossiliferous, low-grade calc-schists,  
215 calcarenites, and limestones of the Pele La Group and the Tang Chu Group (Hughes et al., 2011;  
216 Long and McQuarrie, 2010; Tangri and Pande, 1995), similar to basal TSS lithologies  
217 widespread in the Himalaya and southern Tibet (Dèzes et al., 1999; Gansser, 1964; Hodges et al.,  
218 1996; Le Fort, 1975; Searle and Godin, 2003; Searle et al., 2003). The rocks mapped as GHS  
219 throughout Bhutan comprise Proterozoic-Ordovician(?) granitic and migmatitic orthogneiss,  
220 migmatitic metasedimentary rocks, schist, paragneiss, quartzite, and discrete marble bands,  
221 pervasively intruded by Miocene leucogranites (Bhargava, 1995; Davidson et al., 1997; Gansser,  
222 1983; Grujic et al., 2002; Hollister and Grujic, 2006; Long and McQuarrie, 2010; Long et al.,  
223 2011c; Swapp and Hollister, 1991). There is little controversy regarding correlations of these

224 rocks with GHS units elsewhere in the Himalaya. Of less certain affinity is a unit interposed  
225 between classically GHS and TSS units referred to as the Chekha Formation (Gansser, 1983;  
226 Jangpangi, 1974; Nautiyal et al., 1964; Tangri and Pande, 1995).

227 The Chekha Formation in Bhutan comprises non-fossiliferous greenschist to amphibolite  
228 facies metapelite, paragneiss, augen gneiss, quartzite and calc-silicate intruded by leucogranite  
229 sills and dikes (Cooper et al., in press; Gansser, 1983; Grujic et al., 2002; Kellett et al., 2009;  
230 Long and McQuarrie, 2010; McQuarrie et al., 2008). Kellett et al. (2009); Kellett et al. (2010);  
231 and Kellett and Grujic (2012) correlated the Chekha regionally with TSS units in other parts of  
232 the Himalaya, notably the Everest Series and North Col Formation of eastern Nepal (Searle et al.,  
233 2003), the Annapurna Yellow Formation of central Nepal (Gleeson and Godin, 2006), and the  
234 Haimanta Group of NW India (Chambers et al., 2009). If this is the case, then age constraints for  
235 these other units suggest a probable Cambrian age for the Chekha (Burchfiel et al., 1992; Carosi  
236 et al., 1999; Colchen et al., 1986; Frank et al., 1973; Lombardo et al., 1993; Mu et al., 1973;  
237 Myrow et al., 2009; Wang and Zhen, 1975). Other workers have used the position of the Chekha  
238 at the base of the TSS and its lack of fossils to infer a Precambrian age (Gansser, 1983; Tangri  
239 and Pande, 1995) for the unit. Detrital zircon U-Pb age spectra from some Chekha samples are  
240 similar to those obtained for TSS samples, whereas others are more like those obtained for GHS  
241 samples collected in Bhutan (Gehrels et al., 2011; Hughes et al., 2011; Long and McQuarrie,  
242 2010; McQuarrie et al., 2008). As Hughes et al. (2011) note, additional stratigraphic constraints  
243 on the depositional age of the Chekha Formation are needed.

244 The contacts between the Chekha Formation and units above and below have been variably  
245 interpreted. Gansser (1983) described the GHS–Chekha contact as conformable and noted that  
246 both the uppermost GHS pelitic units and the lowermost Chekha Formation schists contain

247 distinct biotite porphyroblasts (cross-biotites) lying perpendicular to foliation but parallel to  
248 lineation. Grujic et al. (2002), on the other hand, found evidence for a diffuse top-to-the-north  
249 shear zone (width unconstrained) at the base of the Chekha Formation across Bhutan, and re-  
250 interpreted the Dang Chu (or Tang Chu), Ura, Zhemgang (or Black Mountain), and Sakteng (or  
251 Radi) exposures as klippen soled by the STFS basal detachment. Their main lines of evidence  
252 were: (1) Top-to-the-north shear sense indicators at the top of the GHS and the base of the  
253 Chekha Formation; (2) The presence of migmatite and sillimanite in the GHS that are absent  
254 from the Chekha Formation above; and (3) An upsection decrease in metamorphic grade within  
255 the Chekha Formation. However, despite these first-order observations across Bhutan, no  
256 discrete (meter-scale) brittle-ductile shear zone at the contact, upward increase in strain towards  
257 the contact, or definitive structural discordance between footwall and hanging wall units has yet  
258 been described at this structural level (e.g. Carosi et al., 2006; Grujic et al., 2002; Kellett et al.,  
259 2009), contrary to observations of classic STFS detachments in other parts of the Himalaya (e.g.  
260 Burchfiel et al., 1992; Hodges et al., 1992; Hodges et al., 1996; Pognante and Benna, 1993;  
261 Searle et al., 1997; Searle, 1999; Vannay and Hodges, 1996).

262 The ambiguity in the GHS–Chekha contact is exemplified by the contrasting mapping of two  
263 different groups working in Bhutan, which shows little agreement on either the position or the  
264 nature of the contact. Long and McQuarrie (2010), for example, largely followed the original  
265 mapping by Gansser (1983), and agreed with Grujic et al. (2002) that the base of the Chekha  
266 Formation in the Dang Chu, Ura, and Sakteng klippen was a top-to-the-north shear zone of the  
267 STFS. However, in contrast to Grujic et al. (2002), they suggested that interfingering of GHS  
268 and Chekha units at the base of the Zhemgang klippe in southern Bhutan indicated a depositional  
269 contact there (Figures 2a and 5). Grujic et al. (2011), on the other hand, map the Chekha to a far

270 greater extent throughout central Bhutan, combining the Dang Chu and Zhemgang klippe into a  
271 single entity, and extending the Ura klippe northward, where it is cut by the KT (Figure 2b). A  
272 direct comparison between the maps of the two groups (Figure 2) suggests that the large areal  
273 extent of the Chekha mapped by Grujic et al. (2012) corresponds closely to the extent of the  
274 GHS metasedimentary unit mapped by Long and McQuarrie (Figure 5). This again reinforces the  
275 ambiguity between the two lithologic units and suggests that new data is needed to understand  
276 the structural relationship between them.

277 The difference in mapping of the STFS in central Bhutan has implications for the magnitude  
278 of displacement on the STFS. The interpretation by Long and McQuarrie (2010) that the base of  
279 the Zhemgang klippe is a conformable contact between GHS and TSS units but the base of the  
280 Ura klippe is a strand of the STFS led them to argue that the breakaway zone for the STFS must  
281 lie in between the two (Figures 2a and 3a). If this is the case then it limits slip on the STFS to a  
282 maximum of only 20 km, and reduces the significance of extensional faulting as a major orogen-  
283 building process. In contrast, mapping of STFS detachments (including at the base of the  
284 Zhemgang klippe) by Grujic et al. (2012) as far as 100 km south of the main STFS trace along  
285 the Himalayan range crest, with no observed breakaway zone, means that STFS hanging-wall-  
286 on-footwall relationships can be traced in the direction of slip for ca. 100 km, implying large  
287 displacements on this system.

288 Thermobarometric studies across the GHS–Chekha contact in Bhutan are limited. Studies by  
289 Davidson et al. (1997) and Daniel et al. (2003) found the GHS to have reached peak  
290 metamorphic temperatures of 600–750°C and pressures of 8–10 kbar. In a detailed  
291 thermobarometric study across the Ura klippe based on silicate mineral compositions, Kellett et  
292 al. (2010) infer a change in temperature across the GHS–Chekha contact, but see no discernable

293 change in pressure. On closer inspection, their data show a similarly large spread in pressure-  
294 temperature (*P-T*) conditions for both the Chekha Formation (576–730°C and 6.9–8.7 kbar) and  
295 the GHS (560–789°C and 8.0–9.1 kbar), indicating no metamorphic discontinuity across this  
296 contact. Their results are similar in the Jomolhari region of NW Bhutan (referred to by the  
297 authors as the Lingshi klippe), where one sample from the base of the Chekha Formation gives a  
298 *P-T* of 721°C and 8.7 kbar, while 6 samples from the GHS give a spread of 622–787°C and 6.2–  
299 10.9 kbar. Thermobarometric data from a recent study across the GHS-Chekha contact at the  
300 base of the Zhemgang klippe by Corrie et al. (2012) supports the interpretation of Long and  
301 McQuarrie (2010) that it is a conformable contact, noting a gradual change in peak temperature  
302 and pressure across the contact from ca. 540–620°C and 9 kbar in the GHS approximately 2 km  
303 from the contact to 550°C and 7.5 kbar throughout the Chekha Formation. In the only other  
304 RSCM study in Bhutan to date, Kellett and Grujic (2012) obtained peak RSCM temperatures  
305 from Chekha and TSS rocks of the Lingshi klippe that show little variation, with a consistently  
306 low peak temperature of ca. 300°C. By combining these RSCM data with the *P-T* data of Kellett  
307 et al. (2010), Kellett and Grujic (2012) inferred a gradual change in temperature across the GHS–  
308 Chekha contact, which they ascribed to a diffuse shear zone at this structural level. However, the  
309 substantial drop in temperature to ca. 300°C is approximately 600 m above this contact,  
310 suggesting a more significant offset at a structurally higher position.

311 The nature of the contact between the Chekha Formation and the overlying indisputable TSS  
312 (Pele La Group and Tang Chu Group) is also unclear. Exposed in the Mount Jomolhari region in  
313 NW Bhutan and in the Dang Chu klippe (We refer to it as such because it is cut by the Dang Chu  
314 river. It is usually referred to as the Tang Chu klippe after Gansser (1983), but this is a potential  
315 source of confusion because the Tang Chu actually river lies to the east near the Ura klippe) in

316 central Bhutan, Gansser (1983) and Carosi et al. (2006) mapped it as a conformable contact, but  
317 Edwards et al. (1996), Hollister and Grujic (2006), and Chambers et al. (2011) interpreted it as  
318 an STFS detachment. In NW Bhutan (Figure 1), Cooper et al. (in press) mapped recumbently  
319 folded fossiliferous marbles of the TSS above amphibolite facies metapelites, calc-silicates, and  
320 leucogranites of the Chekha Formation. The abrupt change in structural style across the contact  
321 between these two units together with the stark change in lithology and metamorphic grade led  
322 the authors to interpret this contact as a detachment of the STFS.

323 In the Dang Chu klippe, Gansser (1983) mapped two isolated exposures of the TSS lying  
324 above the Chekha Formation. In the more accessible northern exposure, the transition from  
325 Chekha Formation to TSS units of the Pele La Group and Tang Chu Group is marked by a  
326 dramatic change in structural style from foliated metapelites and quartzites to recumbently folded  
327 calc-silicates and marbles (Figure 4a-c). Just to the east of the southern TSS exposure mapped by  
328 Gansser (1983), Hughes et al. (2011) identified Cambrian brachiopod and trilobite fossils in  
329 siliciclastic and carbonate units of the Pele La Group. Although this location has been mapped by  
330 other researchers as part of the Chekha Formation (Grujic et al., 2002; Grujic et al., 2011; Kellett  
331 et al., 2009; Kellett et al., 2010; Long and McQuarrie, 2010; Long et al., 2011c), we join Hughes  
332 et al. (2011) as interpreting these fossiliferous outcrops as part of the TSS and have extended the  
333 southern exposure of this unit in the Dang Chu klippe eastward to include this locality (Figure 1).

334 Above the Chekha Formation in the center of the Zhemgang klippe (Figure 4e), Long and  
335 McQuarrie (2010) mapped the Maneting Formation, a biotite-garnet bearing phyllitic unit  
336 (Figure 4f) of the Pele La group (Tangri and Pande, 1995). Based on an observed upsection  
337 transition from Chekha quartzite to Maneting phyllite and interfingering of the two lithologies,  
338 they interpreted the contact between the Chekha and Maneting Formations to be conformable



339 (Figures 2a and 5). Thermobarometric data from Corrie et al. (2012) agree with this  
340 interpretation, suggesting a steady decrease in peak  $P$ - $T$  conditions across the Chekha-Maneting  
341 contact, with no evidence for a structural break.

342 Because structural studies alone do not seem sufficient to determine the nature of the GHS–  
343 Chekha and Chekha–TSS contacts in the central latitudes of Bhutan, we applied thermometric  
344 techniques to evaluate the evidence for a metamorphic discontinuity across them. Although  
345 conventional pelitic thermobarometers are easily applied to many GHS rocks, Chekha Formation  
346 and TSS rocks typically contain less suitable high-variance mineral assemblages. As a  
347 consequence, we focused our studies on the establishment of peak metamorphic temperatures  
348 through the more widely-applicable Raman spectroscopy on carbonaceous material (RSCM)  
349 method. This relatively new technique (Aoya et al., 2010; Beyssac et al., 2002a; Beyssac et al.,  
350 2002b; Rahl et al., 2005) has become very popular in recent years and has been applied to rocks  
351 from several sectors of the Himalayan orogen (Beyssac et al., 2004; Bollinger et al., 2004;  
352 Célérier et al., 2009; Cottle et al., 2011; Kellett and Grujic, 2012). The popularity of the RSCM  
353 thermometer stems from its applicability to rocks of many bulk compositions, the fact that it is  
354 apparently independent of metamorphic pressure (unlike most of the commonly used  
355 metamorphic thermometers for amphibolite facies metamorphic rocks), and its resistance to  
356 retrograde resetting during protracted or polyphase metamorphism.

357

### 358 **RSCM THERMOMETRY**

359 Carbonaceous material (CM) is a common constituent of metasedimentary rocks, deriving from  
360 the solid-state metamorphic transformation of original organic material (Buseck and Huang,  
361 1985). During diagenesis and metamorphism this CM experiences progressive structural

362 organization until it transforms into graphite. The degree of organization is independent of  
363 pressure but strongly dependent on temperature such that the CM can be used as an indicator of  
364 metamorphic grade (Beysac et al., 2002a; Beysac et al., 2002b; Rietmeijer and Mackinnon,  
365 1985; Wopenka and Pasteris, 1993). Beysac et al. (2002a) demonstrated that peak metamorphic  
366 temperature ( $T$ ) can be estimated in the range 330–650°C with a nominal uncertainty of  $\pm 50^\circ\text{C}$   
367 ( $1\sigma$ ) by measuring the peak area ratio ( $R_2$ ) of characteristic CM bands (D1, D2, G: Figure 6) in  
368 the Raman spectrum and inputting this parameter into the equation:  $T(^{\circ}\text{C}) = -445 R_2 + 641$ .

369 Rahl et al. (2005) devised an alternative calibration of the RSCM thermometer that extends its  
370 range to 100–700°C. In this calibration, peak metamorphic temperature is calculated from both  
371 the peak area ratio ( $R_2$ ) of Beysac et al. (2002a) and the peak height ratio ( $R_1$ ) of CM bands D1  
372 and G. Temperature is calculated using the equation:  $T(^{\circ}\text{C}) = 737.3 + 320.9 R_1 - 1067 R_2 -$   
373  $80.638 R_1^2$ . However, both of these calibrations were made using a micro-Raman system with a  
374 514 nm wavelength laser. At Arizona State University we use a 532 nm laser, which results in a  
375 slightly, but systematically larger  $R_2$  ratio than that of a 514.5 nm laser (Aoya et al., 2010). To  
376 account for this difference, Aoya et al. (2010) derived a new 532 nm laser calibration in which  
377 the temperature is calculated using the equation:  $T(^{\circ}\text{C}) = 221.0 R_2^2 - 637.1 R_2 + 672.3$ , where  
378 the  $R_2$  ratio derives from the original Beysac et al. (2002a) calibration. The Aoya et al. (2010)  
379 calibration is valid for samples in the range 340–655°C and we use this for all of our RSCM  
380 calculations.

381

## 382 **Sampling and analysis**

383 We collected 17 samples for RSCM analysis across the Dang Chu klippe, the Ura klippe, and  
384 the Zhemgang klippe, encompassing rocks of the GHS, Chekha Formation, and TSS (Figure 2).

385 Lithologies include paragneiss, pelitic schist, calc-silicate, slate, phyllite, and marble (Table 1).  
386 Laser Raman analyses of CM were made on microprobe-quality polished petrographic thin  
387 sections. In order to avoid variations in mineral orientation and anisotropy on the Raman spectra  
388 (Beyssac et al., 2002a; Katagiri et al., 1988), thin sections were cut normal to foliation and  
389 parallel to stretching lineation (when present).

390 Measurements were made using a custom-built Raman spectrometer in the LeRoy Eyring  
391 Center for Solid State Science at Arizona State University. The sample was excited using a  
392 Coherent *Compass* laser, with power controlled using neutral density filters. The laser was  
393 focused onto the sample using a  $\times 50$  Mitutoyo objective, and the signal was discriminated from  
394 the laser excitation with a Kaiser laser band pass filter followed by a Semrock edge filter. The  
395 system has a spectral resolution of  $3.5 \text{ cm}^{-1}$  using a  $1200 \text{ g/mm}$  grating and a spatial resolution of  
396  $<1 \text{ }\mu\text{m}$  with the  $\times 50$  objective lens. In order to avoid any mechanical disruption of the CM from  
397 the thin section making and polishing process (Beyssac et al., 2003), the laser was typically  
398 focused on CM situated beneath the surface of a transparent grain of quartz or calcite (Data  
399 Repository Item A). The data were collected using an Acton 300i spectrograph and a back  
400 thinned Princeton Instruments liquid nitrogen cooled CCD detector. Grains of CM were analyzed  
401 with a 3 mW beam for 120 seconds over a spectral window of 1100 to  $2000 \text{ cm}^{-1}$ . Depending on  
402 the abundance of CM, between 15 and 25 grains were analyzed in each sample in order to  
403 evaluate the degree of in-sample heterogeneity. Peak positions, band areas and band widths of  
404 the resulting Raman spectra were determined with the computer program PeakFit 4.12 (Systat  
405 Software Inc.).

406

407 **Results**

408 All temperatures were calculated using the 532 nm laser calibration of Aoya et al. (2010) and are  
409 given in Table 1. For comparison, we also calculated temperatures with the Beyssac et al.  
410 (2002b) and Rahl et al. (2005) 514 nm laser calibrations, which gave results in close agreement  
411 (Data Repository Item B). Examples of Raman spectra for each sample are shown in Figure 6  
412 together with R2 values and calculated temperatures. Photographs of representative CM grains  
413 from selected samples can be found in Data Repository Item A.

414 In Table 1, the variation in R2 within each sample is indicated by the standard deviation ( $1\sigma$ ).  
415 CM heterogeneity can result from differences in the original organic material, variations in the  
416 structure of the CM, the influence of the mineral matrix (e.g. shielding of CM within  
417 porphyroclasts), or the composition of metamorphic fluids (Beyssac et al., 2002a; Beyssac et al.,  
418 2002b; Large et al., 1994). The average variation in R2 for the 17 samples is 0.095, which  
419 corresponds to a temperature difference of  $\pm 50^\circ\text{C}$ . Sample FB132 has the highest variation in R2  
420 at  $\pm 0.122$ , which corresponds to a temperature difference of  $\pm 75^\circ\text{C}$ .

421 Temperatures calculated using the calibration of Aoya et al. (2010) are reported as standard  
422 means of multiple measurements from each sample. The internal uncertainty on our analytical  
423 procedures is reflected by the variation in temperature within each sample, and is reported as 1  
424 standard deviation on the mean. However, for each individual value of R2, there is also an  
425 associated external uncertainty on the calculated temperature of  $\pm 50^\circ\text{C}$  stemming from the  
426 original calibration of CM organization against independent  $P$ - $T$  data (Beyssac et al., 2002a).  
427 Therefore, in order to report a complete and more accurate uncertainty, we added our internal  
428 and external uncertainties in quadrature before dividing by the square root of the number of  
429 analyses per sample. Final temperatures are thus reported at 2 standard errors of the mean (Table  
430 1 and Data Repository Item B).

431 Thirteen samples from Chekha and GHS units give very consistent temperatures, with an  
432 error-weighted mean average of  $560 \pm 2^\circ\text{C}$  (2SE) (Figures 2, 7, and 9). The only change in peak  
433 temperature is seen in four samples across the Dang Chu klippe. Two foliated calc-silicates on  
434 the NW edge of the klippe, samples FB64, and FB85, give slightly lower peak temperatures of  
435  $508 \pm 33^\circ\text{C}$  and  $489 \pm 26^\circ\text{C}$ , respectively. The lowest temperatures are seen in samples FB28, a  
436 folded marble collected at Pele La within the northern TSS exposure (Figure 4b), and FB77, a  
437 black slate located on the W side of the klippe in the Chekha Formation. These give temperatures  
438  $130\text{--}140^\circ\text{C}$  lower than the majority of the samples at  $430 \pm 30^\circ\text{C}$  and  $420 \pm 21^\circ\text{C}$ , respectively.

439

#### 440 **Comparison with GARB-GMBP thermometry**

441 In order to verify the temperatures calculated with the RSCM method, we conducted independent  
442 *P-T* calculations on three of the 17 samples. Samples FB07, FB125, and FB132 have a mineral  
443 assemblage of garnet + biotite + muscovite + plagioclase, permitting the application of the well-  
444 established GARB (garnet-biotite) exchange thermometer (Ferry and Spear, 1978) and GMBP  
445 (garnet-muscovite-biotite-plagioclase) net-transfer barometer (Ghent and Stout, 1981). In order  
446 to minimize sources of uncertainty in the thermobarometric calculations, we followed the  
447 approach of Cooper et al. (2010) by characterizing textural and geochemical relationships in  
448 detail and conducting multiple independent calculations on each sample. For more details, see  
449 Data Repository Item C.

450 Mineral composition data were obtained with a JEOL JXA-8200 electron microprobe at the  
451 University of California, Los Angeles and a Cameca SX50 electron microprobe at the University  
452 of Massachusetts. Thermobarometric calculations were made using THERMOCALC v. 3.33  
453 software (Powell and Holland, 1988), and the latest version of the Holland and Powell data set

454 (Holland and Powell, 1998). Activity-composition relationships were calculated using the AX  
455 program (Tim Holland: <http://www.esc.cam.ac.uk/research/research-groups/holland/ax>).  
456 Individual *P-T* calculations and representative mineral analyses can be found in Data Repository  
457 Items D and E.

458 RSCM temperatures and GARB-GMBP temperatures and pressures for each sample are given  
459 in Table 2 for comparison. The results show that there is good agreement between the three  
460 independent temperature measurements within the limits of the uncertainties on both methods  
461 and the pressure estimates on the three samples are also consistent, with an error-weighted mean  
462 pressure of  $5.2 \pm 0.5$  kbar (2SE).

463

#### 464 **IMPLICATIONS FOR THE STFS IN CENTRAL BHUTAN**

465 The lack of either a distinct discontinuity or a progressive change in temperature across the base  
466 of both the Dang Chu and Ura klippen, and similar temperatures in the center of the Zhemgang  
467 klippe raises questions about the interpretation of the GHS–Chekha contact being a strand of the  
468 STFS. In contrast, the lower peak temperatures reached by four samples in the Dang Chu klippe  
469 point to a likely detachment between the Chekha Formation and overlying TSS sediments, an  
470 interpretation supported by the change in structural style observed in rocks above and below the  
471 contact (Figure 4).

472 The interpretation that there is no structural discontinuity between the GHS and the Chekha  
473 Formation is consistent with the conclusion reached by Long and McQuarrie (2010) that the  
474 Chekha Formation of the Zhemgang klippe (which they interpret as part of the TSS) is in  
475 depositional contact with the GHS (Figures 1 and 2a). However, we disagree with Long and  
476 McQuarrie (2010) regarding the broader tectonic significance of that observation. We suggest

477 that the Chekha Formation and overlying Maneting Formation are in the STFS footwall, and that  
478 the absence of evidence for fault slip at the GHS–Chekha contact in the Zhemgang klippe is not  
479 surprising as a consequence. On the other hand, the TSS units that give low peak temperatures of  
480 420–430°C coincide with recumbently folded marbles that exhibit a wholly different structural  
481 style to both the Chekha and GHS units below (Figure 4). Although we have not found  
482 fossiliferous marbles in the northern TSS Dang Chu exposure, the fossils found to the south by  
483 Hughes et al. (2011) are from the TSS. If similar fossiliferous beds are present in the northern  
484 part of the klippe, they must lie at structurally higher elevations that have so far proved  
485 inaccessible. The strongly foliated, high-strain calc-silicate samples FB64 and FB85, which give  
486 intermediate peak temperatures of ca. 490–510°C, are interpreted as basal units of the TSS that  
487 have been heated and transposed by shearing along the STFS detachment. They therefore  
488 roughly define the position of the STFS shear zone.

489 Figure 8a shows our interpretation for the distribution of RSCM temperatures in central  
490 Bhutan. The Chekha Formation and GHS are combined as one sequence in the figure, although  
491 our data and observations do not speak to whether or not the two are separated by a major  
492 unconformity. We propose a different map pattern for the TSS in the Dang Chu area that  
493 includes the four lower-temperature samples FB28, FB64, FB77 and FB85, and we interpret the  
494 contact between the TSS and structurally lower units to be the sole STFS detachment. The high-  
495 strain calc-silicate samples FB64 and FB85 are mapped at the base of the TSS, and we suggest  
496 that their slightly higher peak temperatures result from shear heating along the STFS shear zone.  
497 This interpretation is consistent with all outcrops we have seen in the area, but the quality of  
498 outcrop is so poor that detailed field confirmation of this map pattern is difficult.

499 If our interpretation is correct, it suggests that to truly understand the kinematics and

500 displacement history of the STFS, we need to focus on this upper contact in the Dang Chu area,  
501 not on the previously mapped GHS–Chekha contacts. Our interpretation is inconsistent with the  
502 contention by Long and McQuarrie (2010) that the stratigraphic contact between TSS and GHS  
503 units in the Zhemgang klippe can be used to place a limit of ca. 20 km on STFS displacement  
504 and thus the magnitude of putative channel flow. The presence of TSS units ca. 80 km south of  
505 the Himalayan range crest suggests that displacement on the STFS may in fact be even greater  
506 than previously thought (Figure 8b).

507 An alternative interpretation of the geology that fits with our data is that of Grujic et al.  
508 (2011), who map the Chekha Formation more extensively across Bhutan (Figure 2b). According  
509 to their mapping, the majority of RSCM samples that give a consistent temperature of ca. 560°C  
510 are situated within the Chekha Formation. The exceptions are samples FB125 and FB132, which  
511 lie within the GHS on the edge of the Dang Chu klippe and samples BT1134, BT1136, and  
512 BT1138, which lie within the Maneting Formation in the Zhemgang klippe. However, we do not  
513 favor their interpretation as we see no evidence for a discrete shear zone at any of the GHS–  
514 Chekha contacts mapped and we have found paragneisses reasonably attributed to the GHS  
515 within areas mapped as Chekha Formation by Grujic et al. (2011) in both the Dang Chu and Ura  
516 klippen. Grujic et al. (2011) also map the TSS very differently in the Dang Chu klippe, with no  
517 clear explanation as to why. The folded marbles at Baylangdra (Figure 4a) are mapped as part of  
518 the TSS but at Pele La (Figure 4b) they are mapped as Chekha. This is inconsistent with both our  
519 temperature and structural data.

520

521 **CONCLUSIONS**



522 RSCM thermometry data from 17 samples combined with structural observations across three  
523 purported STFS klippen in central Bhutan suggest that current maps of this structure require  
524 revision. We find no change in peak metamorphic temperature across the contact between  
525 Chekha Formation rocks and underlying indisputable GHS units. Instead, we see a 130–140°C  
526 drop in temperature across an upper contact between the Chekha Formation and Precambrian-  
527 Devonian(?) TSS sediments of the Pele La and Tang Chu Groups. We therefore see no reason to  
528 infer that the Chekha Formation and the GHS are separated by the basal strand of the STFS. We  
529 regard the upper contact between the Chekha Formation and indisputable TSS units as the sole  
530 STFS detachment, and suggest that future studies of the kinematics and displacement on this  
531 system should be focused on this upper contact. The lack of matching hanging wall and footwall  
532 lithologic units or metamorphic grade in the direction of STFS motion suggests that  
533 displacement on the STFS may be as much as ca. 80 km, not less than ca. 20 km as suggested by  
534 Long and McQuarrie (2010). In light of the new data presented here, there is no clear evidence  
535 for a breakaway zone for the STFS in southern Bhutan.

536

### 537 **ACKNOWLEDGEMENTS**

538 This work was supported by US National Science Foundation grant EAR-0838112 to K.V.H. We  
539 thank Emmanuel Soignard of the LeRoy Eyring Center for Solid State Science at ASU for his  
540 help with the Raman spectrometer, and Frank Kyte at UCLA and Michael Jercinovic at the  
541 University of Massachusetts for their assistance with the electron microprobe analyses. Field  
542 work would not have been possible without assistance from Kelin Whipple and Arjun Heimsath  
543 and the support of our friends and colleagues in Bhutan: Peldon Tshering (National Environment  
544 Commission), Ugyen Wanda (Department of Geology and Mines), Karma Choden and Ugyen

545 Rinzen (Yangphel Adventure Travel). Detailed and constructive reviews by editor Eric Kirby  
546 and two anonymous reviewers are gratefully acknowledged.

547

548 **REFERENCES CITED**

549 Acharyya, S. K., and Sastry, M., 1979, Stratigraphy of the eastern Himalaya: Geological Survey  
550 of India Miscellaneous Publications, v. 41, p. 49-67.

551 Aoya, M., Kouketsu, Y., Endo, S., Shimizu, H., Mizukami, T., Nakamura, D., and Wallis, S.,  
552 2010, Extending the applicability of the Raman carbonaceous-material geothermometer  
553 using data from contact metamorphic rocks: *Journal of Metamorphic Geology*, v. 28, no.  
554 9, p. 895-914, doi: 10.1111/j.1525-1314.2010.00896.x.

555 Beaumont, C., Jamieson, R. A., Nguyen, M. H., and Lee, B., 2001, Himalayan tectonics  
556 explained by extrusion of a low-viscosity crustal channel coupled to focused surface  
557 denudation: *Nature*, v. 414, p. 738-742.

558 Beyssac, O., Bollinger, L., Avouac, J.-P., and Goffé, B., 2004, Thermal metamorphism in the  
559 lesser Himalaya of Nepal determined from Raman spectroscopy of carbonaceous  
560 material: *Earth and Planetary Science Letters*, v. 225, p. 233-241.

561 Beyssac, O., Goffe, B., Chopin, C., and Rouzaud, J., 2002a, Raman spectra of carbonaceous  
562 material in metasediments: a new geothermometer: *Journal of Metamorphic Geology*, v.  
563 20, no. 9, p. 859-871.

564 Beyssac, O., Goffé, B., Petitet, J.-P., Froigneux, E., Moreau, M., and Rouzaud, J.-N., 2003, On  
565 the characterization of disordered and heterogeneous carbonaceous materials by Raman  
566 spectroscopy: *Spectrochimica Acta Part A*, v. 59, p. 2267-2276.

567 Beyssac, O., Rouzaud, J.-N., Goffé, B., Brunet, F., and Chopin, C., 2002b, Graphitization in a  
568 high-pressure, low-temperature metamorphic gradient: a Raman microspectroscopy and  
569 HRTEM study: *Contributions to Mineralogy and Petrology*, v. 143, p. 19-31.

570 Bhargava, O. N., 1995, *The Bhutan Himalaya: A Geological Account*, Geological Society of  
571 India Special Publication, Calcutta, 245 p.

572 Bollinger, L., Avouac, J. P., Beyssac, O., Catlos, E. J., Harrison, T. M., Grove, M., Goffé, B.,  
573 and Sapkota, S., 2004, Thermal structure and exhumation history of the Lesser Himalaya  
574 in central Nepal: *Tectonics*, v. 23, no. 5, p. 1-19, doi: 10.1029/2003TC001564.

575 Brasier, M. D., and Singh, P., 1987, Microfossils and Precambrian-Cambrian boundary  
576 stratigraphy at Maldeota, Lesser Himalaya: *Geological Magazine*, v. 124, p. 323-345.

577 Brookfield, M. E., 1993, The Himalayan passive margin from Precambrian to Cretaceous times:  
578 *Sedimentary Geology*, v. 84, p. 1-35.

579 Brown, R. L., and Nazarchuk, J. H., 1993, Annapurna detachment fault in the Greater Himalaya  
580 of central Nepal, *in* Treloar, P. J., and Searle, M. P., eds., *Himalayan Tectonics*, Volume  
581 74: London, Geological Society Special Publication, p. 461-473, doi:  
582 10.1144/GSL.SP.1993.074.01.31.

583 Burbank, D. W., Beck, R. A., and Mulder, T., 1997, The Himalayan foreland basin, *in* Yin, A.,  
584 and Harrison, M., eds., *The tectonic evolution of Asia*: Cambridge, Cambridge University  
585 Press, p. 149-188.

586 Burchfiel, B. C., Zhiliang, C., Hodges, K. V., Yuping, L., Royden, L. H., Changrong, D., and  
587 Jiene, X., 1992, The South Tibetan Detachment System, Himalayan Orogen: Extension  
588 Contemporaneous With and Parallel to Shortening in a Collisional Mountain Belt, 41 p.

589 Burg, J. P., and Chen, G. M., 1984, Tectonics and structural zonation of southern Tibet, China:  
590 Nature, v. 311, p. 219-223.

591 Buseck, P. R., and Huang, B.-J., 1985, Conversion of carbonaceous material to graphite during  
592 metamorphism: *Geochimica et Cosmochimica Acta*, v. 49, p. 2003-2016.

593 Caby, R., Pêcher, A., and Le Fort, P., 1983, Le grande chevauchement central himalayen:  
594 Nouvelles données sur le métamorphisme inverse à la base de la Dalle du Tibet: *Revue*  
595 *de Géographie Physique et Géologie Dynamique*, v. 24, p. 89-100.

596 Carosi, R., Lombardo, B., Musumeci, G., and Pertusati, P. C., 1999, Geology of the Higher  
597 Himalayan Crystallines in the Khumbu Himal (Eastern Nepal): *Journal of Asian Earth*  
598 *Sciences*, v. 17, p. 785-803.

599 Carosi, R., Molli, B. L., Musumeci, G., and Pertusati, P. C., 1998, The south Tibetan detachment  
600 system in the Rongbuk valley, Everest region: Deformation features and geological  
601 implications: *Journal of Asian Earth Sciences*, v. 16, p. 299-311.

602 Carosi, R., Montomoli, C., Rubatto, D., and Visona, D., 2006, Channel Flow, Ductile Extrusion  
603 and Exhumation in Continental Collision Zones, *in* Law, R., Searle, M., and Godin, L.,  
604 eds., Volume 268, Geological Society London Special Publication, p. 425-444.

605 Célérier, J., Harrison, T. M., Beyssac, O., Herman, F., Dunlap, W. J., and Webb, A. A. G., 2009,  
606 The Kumaun and Garwhal Lesser Himalaya, India: Part 2. Thermal and deformation  
607 histories: *Geological Society of America Bulletin*, v. 121, no. 9/10, p. 1281-1297, doi:  
608 10.1130/B26343.1.

609 Chakungal, J., Dostal, J., Grujic, D., Duchêne, S., and Ghalley, K. S., 2010, Provenance of the  
610 Greater Himalayan sequence: Evidence from mafic granulites and amphibolites in NW  
611 Bhutan: *Tectonophysics*, v. 480, p. 198-212.

612 Chambers, J., Caddick, M., Argles, T., Horstwood, M., Sherlock, S., Harris, N., Parrish, R., and  
613 Ahmad, T., 2009, Empirical constraints on extrusion mechanisms from the upper margin  
614 of an exhumed high-grade orogenic core, Sutlej valley, NW India: *Tectonophysics*, v.  
615 477, p. 77-92.

616 Chambers, J., Parrish, R., Argles, T., Harris, N., and Horstwood, M., 2011, A short duration  
617 pulse of ductile normal shear on the outer South Tibetan detachment in Bhutan:  
618 alternating channel flow and critical taper mechanics of the eastern Himalaya: *Tectonics*,  
619 v. 30, doi: 10.1029/2010TC002784.

620 Colchen, M., LeFort, P., and Pêcher, A., 1986, *Annapurna-Manaslu-Ganesh Himal.*, Paris,  
621 Centre National de la Recherche Scientifique, 136 p.

622 Cooper, F. J., Adams, B. A., Edwards, C. S., and Hodges, K. V., in press, Large normal-sense  
623 displacement on the South Tibetan fault system in the eastern Himalaya: *Geology*, doi:  
624 10.1130/G33318.1.

625 Cooper, F. J., Platt, J. P., Anczkiewicz, R., and Whitehouse, M. J., 2010, Footwall dip of a core  
626 complex detachment fault: thermobarometric constraints from the northern Snake Range  
627 (Basin and Range, USA): *Journal of Metamorphic Geology*, doi: 10.1111/j.1525-  
628 1314.2010.00907.x.

629 Corrie, S. L., Kohn, M. J., McQuarrie, N., and Long, S. P., 2012, Flattening the Bhutan  
630 Himalaya: *Earth and Planetary Science Letters*, v. 349-350, p. 67-74, doi:  
631 10.1016/j.epsl.2012.07.001.

632 Cottle, J., Waters, D., Riley, D., Beyssac, O., and Jessup, M. J., 2011, Metamorphic history of  
633 the South Tibetan Detachment System, Mt. Everest region, revealed by RSCM

634 thermometry and phase equilibria modelling: *Journal of Metamorphic Geology*, v. 29, p.  
635 561-582.

636 Cottle, J. M., Jessup, M. J., Newell, D. L., Searle, M. P., Law, R. D., and Horstwood, M. S. A.,  
637 2007, Structural insights into the early stages of exhumation along an orogen-scale  
638 detachment: The South Tibetan Detachment System, Dzaka Chu section, Eastern  
639 Himalaya: *Journal of structural geology*, v. 29, p. 1781-1797.

640 Critelli, S., and Garzanti, E., 1994, Provenance of the lower Tertiary Murree redbeds (Hazara-  
641 Kashmir syntaxis, Pakistan) and initial rising of the Himalayas: *Sedimentary Geology*, v.  
642 89, p. 265-284.

643 Daniel, C. G., Hollister, L. S., Parrish, R., and Grujic, D., 2003, Exhumation of the Main Central  
644 Thrust from Lower Crustal Depths, Eastern Bhutan Himalaya: *Journal of Metamorphic  
645 Geology*, v. 21, p. 317--334.

646 Davidson, C., Grujic, D. E., Hollister, L. S., and Schmid, M., 1997, Metamorphic reactions  
647 related to decompression and synkinematic intrusion of leucogranite, High Himalayan  
648 Crystallines, Bhutan: *Journal of Metmorphic Geology*, v. 15, p. 593-612.

649 de Sigoyer, J., Chavagnac, V., Blichert-Toft, J., Villa, I. M., Luais, B., Guillot, S., Cosca, M.,  
650 and Mascle, G., 2000, Dating the Indian continental subduction and collisional thickening  
651 in the northwest Himalaya: multichronology of the Tso Morari eclogites: *Geology*, v. 28,  
652 p. 487-490.

653 DeCelles, P. G., Gehrels, G. E., and Quade, J., 1998, Eocene-early Miocene foreland basin  
654 development and the history of Himalayan thrusting, western and central Nepal:  
655 *Tectonics*, v. 17, p. 741-765.

656 Dèzes, P. J., Vannay, J.-C., Steck, A., Bussy, F., and Cosca, M., 1999, Synorogenic extension;  
657 quantitative constraints on the age and displacement of the Zaskar shear zone (northwest  
658 Himalaya): *Geological Society of America Bulletin*, v. 111, no. 3, p. 364-374.

659 Edwards, M., Kidd, W., Li, J., Yue, Y., and Clark, M., 1996, Multi-stage development of the  
660 southern Tibetan detachment system near Khula Kangri. New data from Gonto La:  
661 *Tectonophysics*, v. 260, p. 1-19.

662 Edwards, M., Pêcher, A., Kidd, W., Burchfiel, B., and Royden, L., 1999, Southern Tibet  
663 Detachment System at Khula Kangri, Eastern Himalaya: A Large-Area, Shallow  
664 Detachment Stretching into Bhutan?: *The Journal of Geology*, v. 107, p. 623-631.

665 Edwards, M. A., and Harrison, T. M., 1997, When did the roof collapse? Late Miocene north-  
666 south extension in the high Himalaya revealed by Th-Pb monazite dating of the Khula  
667 Kangri granite: *Geology*, v. 25, no. 6, p. 543-546.

668 Ferry, J. M., and Spear, F. S., 1978, Experimental calibration of the partitioning of Fe and Mg  
669 between biotite and garnet: *Contributions to Mineralogy and Petrology*, v. 66-2, p. 113-  
670 117.

671 Frank, W., Hoinkes, G., Miller, C., Purtscheller, F., Richter, W., and Thöni, M., 1973, Relations  
672 between metamorphism and orogeny in a typical section of the Indian Himalayas:  
673 *Mineralogy and Petrology*, v. 20, p. 303-332.

674 Gaetani, M., and Garzanti, E., 1991, Multicyclic history of the northern India continental margin  
675 (Northwestern Himalaya): *American Association of Petroleum Geologists Bulletin*, v. 75,  
676 p. 1427-1446.

677 Gansser, A., 1964, *Geology of the Himalayas*, Wiley Interscience, London, 289 p.

678 Gansser, A., 1983, *Geology of the Bhutan Himalaya*, Birkhauser Verlag, Basel, 181 p.

679 Gehrels, G., Kapp, P., DeCelles, P., Pullen, A., Blakey, R., Weislogel, A., Ding, L., Guynn, J.,  
680 Martin, A., McQuarrie, N., and Yin, A., 2011, Detrital zircon geochronology of pre-  
681 Tertiary strata in the Tibetan-Himalayan orogen: *Tectonics*, v. 30, no. TC5016, doi:  
682 10.1029/2011TC002868.

683 Gehrels, G. E., DeCelles, P. G., Martin, A., Ojha, T. P., Pinhassi, G., and Upreti, B. N., 2003,  
684 Initiation of the Himalayan orogen as an early Paleozoic thin-skinned thrust belt:  
685 *Geological Society of America Today*, v. 13, no. 9, p. 4-9.

686 Ghent, E. D., and Stout, M. Z., 1981, Geobarometry and geothermometry of plagioclase-biotite-  
687 garnet-muscovite assemblages: *Contributions to Mineralogy and Petrology*, v. 76-1, p.  
688 92-97.

689 Gleeson, T. P., and Godin, L., 2006, The Chako antiform: a folded segment of the Greater  
690 Himalayan sequence, Nar Valley, Central Nepal Himalaya: *Journal of Asian Earth*  
691 *Sciences*, v. 27, p. 717-734.

692 Godin, L., Grujic, D., Law, R. D., and Searle, M. P., 2006, Crustal flow, extrusion, and  
693 exhumation in continental collision zones: an introduction, *in* Law, R., Searle, M., and  
694 Godin, L., eds., *Channel Flow, Ductile Extrusion and Exhumation in Continental*  
695 *Collision Zones*, Volume 268, Geological Society London Special Publication, p. 1-28.

696 Grujic, D., Coutand, I., Bookhagen, B., Bonnet, S., Blythe, A., and Duncan, C., 2006, Climatic  
697 forcing of erosion, landscape, and tectonics in the Bhutan Himalayas: *Geology*, v. 34, no.  
698 10, p. 801-804.

699 Grujic, D., Hollister, L. S., and Parrish, R. R., 2002, Himalayan metamorphic sequence as an  
700 orogenic channel: insight from Bhutan: *Earth and Planetary Science Letters*, v. 198, p.  
701 177-191.



702 Grujic, D., Warren, C. J., and Wooden, J. L., 2011, Rapid synconvergent exhumation of  
703 Miocene-aged lower orogenic crust in the eastern Himalaya: *Lithosphere*, v. 3, no. 5, p.  
704 346-366.

705 Guillot, S., Hodges, K. V., Le Fort, P., and Pêcher, A., 1994, New constraints on the age of the  
706 Manaslu leucogranite: Evidence for episodic tectonic denudation in the central  
707 Himalayas: *Geology*, v. 22, p. 559-562.

708 Guillot, S., Mahéo, G., de Sigoyer, J., Hattori, K. H., and Pêcher, A., 2008, Tethyan and Indian  
709 subduction viewed from the Himalayan high- to ultrahigh-pressure metamorphic rocks:  
710 *Tectonophysics*, v. 451, no. 1-4, p. 225-241.

711 Heim, A., and Gansser, A., 1939, Central Himalaya--Geological observations of Swiss  
712 expedition, 1936: *Mémoire Société Helvétique Science Naturelle*, v. 73, p. 1-245.

713 Herren, E., 1987, Zaskar shear zone; northeast-southwest extension within the Higher  
714 Himalayas (Ladakh, India): *Geology*, v. 15, p. 409-413.

715 Hodges, K., Bowring, S., Davidek, K., Hawkins, D., and Krol, M., 1998, Evidence for rapid  
716 displacement on Himalayan normal faults and the importance of tectonic denudation in  
717 the evolution of mountain ranges: *Geology*, v. 26, no. 6, p. 483-486.

718 Hodges, K., Hames, W., Olszewski, W., Burchfiel, B., Royden, L., and Chen, Z., 1994,  
719 Thermobarometric and  $^{40}\text{Ar}/^{39}\text{Ar}$  geochronologic constraints on Eohimalayan  
720 metamorphism in the Dinggye area, southern Tibet: *Contributions to Mineralogy and*  
721 *Petrology*, v. 117, p. 151-163.

722 Hodges, K., Hurtado, J., and Whipple, K., 2001, Southward extrusion of Tibetan crust and its  
723 effect on Himalayan tectonics: *Tectonics*, v. 20, no. 6, p. 799-809.

724 Hodges, K., Parrish, R., Housh, T., Lux, D., Burchfiel, B., Royden, L., and Chen, Z., 1992,  
725 Simultaneous Miocene Extension and Shortening in the Himalayan Orogen: *Science*, v.  
726 258, p. 1466-1470.

727 Hodges, K. V., 2000, Tectonics of the Himalaya and southern Tibet from two perspectives:  
728 *Geological Society of America Bulletin*, v. 112, no. 3, p. 324-350.

729 Hodges, K. V., Burchfiel, B. C., Royden, L. H., Chen, Z., and Liu, Y., 1993, The metamorphic  
730 signature of contemporaneous extension and shortening in the central Himalayan orogen:  
731 Data from the Nyalam transect, southern Tibet: *Journal of Metamorphic Geology*, v. 11,  
732 p. 721-737.

733 Hodges, K. V., Parrish, R. R., and Searle, M. P., 1996, Tectonic evolution of the central  
734 Annapurna Range, Nepalese Himalayas: *Tectonics*, v. 15, no. 6, p. 1264-1291.

735 Holland, T. J. B., and Powell, R., 1998, An internally consistent thermodynamic data set for  
736 phases of petrological interest: *Journal of Metamorphic Geology*, v. 16, p. 309-343.

737 Hollister, L. S., and Grujic, D., 2006, Pulsed channel flow in Bhutan, *in* Law, R., Searle, M., and  
738 Godin, L., eds., *Channel Flow, Ductile Extrusion and Exhumation in Continental*  
739 *Collision Zones*, Geological Society London Special Publication, p. 415-423.

740 Hubbard, M. S., and Harrison, T. M., 1989,  $^{40}\text{Ar}/^{39}\text{Ar}$  age constraints on deformation and  
741 metamorphism in the Main Central thrust zone and Tibetan slab, eastern Nepal Himalaya:  
742 *Tectonics*, v. 8, p. 865-880.

743 Hughes, N. C., Myrow, P. M., McKenzie, N. R., Harper, D. A. T., Bhargava, O. N., Tangri, S.  
744 K., Ghalley, K. S., and Fanning, C. M., 2011, Cambrian rocks and faunas of the Wachi  
745 La, Black Mountains, Bhutan: *Geological Magazine*, v. 148, no. 3, p. 351-379.

746 Jangpangi, B. S., 1974, Stratigraphy and tectonics of parts of eastern Bhutan: Himalayan  
747 Geology, v. 4, p. 139-147.

748 Katagiri, G., Ishida, H., and Ishitani, A., 1988, Raman spectra of graphite edge planes: Carbon,  
749 v. 26, no. 4, p. 565--571.

750 Kellett, D., Grujic, D., and Erdmann, S., 2009, Miocene structural reorganization of the South  
751 Tibetan detachment, eastern Himalaya: Implications for continental collision:  
752 Lithosphere, v. 1, no. 5, p. 259-281.

753 Kellett, D., Grujic, D., Warren, C., Cottle, J., Jamieson, R., and Tenzin, T., 2010, Metamorphic  
754 history of a syn-convergent orogen-parallel detachment: The South Tibetan detachment  
755 system, Bhutan Himalaya: Journal of Metamorphic Geology.

756 Kellett, D. A., and Grujic, D., 2012, New insight into the South Tibetan detachment system: Not  
757 a single progressive deformation: Tectonics, v. 31, no. TC2007, doi:  
758 10.1029/2011TC002957.

759 Large, D. J., Christy, A. G., and Fallick, A. E., 1994, Poorly crystalline carbonaceous matter in  
760 high grade metasediments: implications of graphitization and metamorphic fluids  
761 compositions: Contributions to Mineralogy and Petrology, v. 116, p. 108-116.

762 Law, R., Searle, M., and Godin, L., 2006, Channel Flow, Ductile Extrusion and Exhumation in  
763 Continental Collision Zones, Geological Society London Special Publication, 632 p.

764 Law, R. D., Jessup, M. J., Searle, M. P., Francis, M. K., Waters, D. J., and Cottle, J. M., 2011,  
765 Telescoping of isotherms beneath the South Tibetan Detachment System, Mount Everest  
766 Massif: Journal of Structural Geology, v. 33, p. 1569-1594, doi:  
767 10.1016/j.jsg.2011.09.004.

768 Le Fort, P., 1975, Himalayas: The collided range. Present knowledge of the continental arc:  
769 American Journal of Science, v. 275-A, p. 1-44.

770 Leech, M. L., Singh, S., Jain, A. K., Klemperer, S. L., and Manickavasagam, R. M., 2005, The  
771 onset of India-Asia continental collision: Early, steep subduction required by the timing  
772 of UHP metamorphism in the western Himalaya: Earth and Planetary Science Letters, v.  
773 234, p. 83-97.

774 Lister, G. S., and Snoke, A. W., 1984, S-C mylonites: Journal of Structural Geology, v. 6, p. 617-  
775 638.

776 Lombardo, B., Pertusati, P., and Borghi, S., 1993, Geology and tectonomagmatic evolution of  
777 the eastern Himalaya along the Chomolungma-Makalu transect, *in* Treloar, P. J., and  
778 Searle, M. P., eds., Himalayan Tectonics, Volume 74, Geological Society Special  
779 Publication, p. 341-355.

780 Long, S., and McQuarrie, N., 2010, Placing limits on channel flow: Insights from the Bhutan  
781 Himalaya: Earth and Planetary Science Letters, v. 290, p. 375-390.

782 Long, S., McQuarrie, N., Tobgay, T., and Grujic, D., 2011a, Geometry and crustal shortening of  
783 the Himalayan fold-thrust belt, eastern and central Bhutan: Geological Society of  
784 America Bulletin, doi: 10.1130/B30203.1.

785 Long, S., McQuarrie, N., Tobgay, T., Rose, C., Gehrels, G., and Grujic, D., 2011b,  
786 Tectonostratigraphy of the Lesser Himalaya of Bhutan: Implications for the along-strike  
787 stratigraphic continuity of the northern Indian margin: Geological Society of America  
788 Bulletin.

789 Long, S. P., McQuarrie, N., Tobgay, T., Grujic, D., and Hollister, L., 2011c, Geologic map of  
790 Bhutan: The Journal of Maps, v. 2011, p. 184-192, doi: 10.4113/jom.2011.1159.

791 McQuarrie, N., Robinson, D., Long, S., Tobgay, T., Grujic, D., Gehrels, G., and Ducea, M.,  
792 2008, Preliminary stratigraphic and structural architecture of Bhutan: Implications for the  
793 along strike architecture of the Himalayan system: *Earth and Planetary Science Letters*, v.  
794 272, p. 105-117, doi: 10.1016/j.epsl.2008.04.030.

795 Mu, A. T., Wen, S. H., Wang, Y. K., Chang, P. K., and Yin, C. H., 1973, Stratigraphy of the  
796 Mount Jolmo Lungma region in Southern Tibet, China: *Scientia Sinica*, v. 16, p. 96-111.

797 Myrow, P. M., Hughes, N. C., Searle, M. P., Fanning, C. M., Peng, S.-C., and Parcha, S. K.,  
798 2009, Stratigraphic correlation of Cambrian-Ordovician deposits along the Himalaya:  
799 Implications for the age and nature of rocks in the Mount Everest region: *Geological*  
800 *Society of America Bulletin*, v. 120, no. 3/4, p. 323-332, doi: 10.1130/B26384.1.

801 Najman, Y., Clift, P., Johnson, M. R. W., and Robertson, A. H. F., 1993, Early stages of foreland  
802 basin evolution in the Lesser Himalaya, N India, *in* Treloar, P. J., and Searle, M. P., eds.,  
803 Himalayan tectonics, Volume 74, Geological Society of London Special Publication p.  
804 541-558.

805 Najman, Y. M. R., Pringle, M. S., Johnson, M. R. W., A.H.F., R., and Wijbrans, J. R., 1997,  
806 Laser  $^{40}\text{Ar}/^{39}\text{Ar}$  dating of single detrital muscovite grains from early foreland basin  
807 deposits in India: Implications for early Himalayan evolution: *Geological Society of*  
808 *America Special Paper*, v. 232, p. 243-264.

809 Nautiyal, S. P., Jangpangi, B. S., Singh, P., Guha Sarkar, T. K., Bhate, V. D., Raghavan, M. R.,  
810 and Sahai, T. N., 1964, A preliminary note on the geology of the Bhutan Himalaya:  
811 Report of the 22nd International Geologic Congress, New Delhi, v. 11, p. 1-14.

812 Nelson, K. D., Zhao, W., Brown, L. D., Kuo, J., Che, J., Xianwen, L., Klemperer, S., Makovsky,  
813 Y., Meissner, R., Mechie, J., Kind, R., Wenzel, F., Ni, J., Nabelek, J., Chen, L., Handong,

814 T., Wenbo, W., Jones, A. G., Booker, J., Unsworth, M., Kidd, W. S. F., Hauk, M.,  
815 Alsdorf, D., Ross, A., Cogan, M., Wu, C., Sandvol, E. A., and Edwards, M., 1996,  
816 Partially molten middle crust beneath southern Tibet: Synthesis of Project INDEPTH  
817 Results: *Science*, v. 274, p. 1684-1688.

818 Parrish, R. R., and Hodges, K. V., 1996, Isotopic constraints on the age and provenance of the  
819 Lesser and Greater Himalayan sequences, Nepalese Himalaya: *Geological Society of  
820 America Bulletin*, v. 108, p. 904-911.

821 Pêcher, A., 1991, The contact between the higher Himalaya crystallines and the Tibetan  
822 sedimentary series: Miocene large-scale dextral shearing: *Tectonics*, v. 10, no. 3, p. 587-  
823 598.

824 Pognante, U., and Benna, P., 1993, Dynamics of orogenic wedges and the uplift of high-pressure  
825 metamorphic rocks: *Geological Society of London Special Publication*, v. 74, p. 323-340.

826 Powell, R., and Holland, T. J. B., 1988, An internally consistent dataset with uncertainties and  
827 correlations: 3. Applications to geobarometry, worked examples and a computer  
828 program: *Journal of Metamorphic Geology*, v. 6, p. 173-204.

829 Rahl, J. M., Anderson, K. M., Brandon, M. T., and Fassoulas, C., 2005, Raman spectroscopic  
830 carbonaceous material thermometry of low-grade metamorphic rocks: Calibration and  
831 application to tectonic exhumation in Crete, Greece: *Earth and Planetary Science Letters*,  
832 v. 240, p. 339-354.

833 Rietmeijer, F. J. M., and Mackinnon, I. D. R., 1985, Poorly graphitized carbon as a new  
834 cosmo-thermometer for primitive extraterrestrial materials: *Nature*, v. 316, p. 733-736.

835 Robinson, D. M., DeCelles, P. G., and Copeland, P., 2006, Tectonic evolution of the Himalayan  
836 thrust belt in western Nepal: implications for channel flow models: Geological Society of  
837 America Bulletin, v. 118, p. 865-885.

838 Rowley, D. B., 1996, Age of initiation of collision between India and Asia: A review of  
839 stratigraphic data: Earth and Planetary Science Letters, v. 145, p. 1-13.

840 Searle, M., and Godin, L., 2003, The South Tibetan Detachment and the Manaslu Leucogranite:  
841 A Structural Reinterpretation and Restoration of the Annapurna-Manaslu Himalaya,  
842 Nepal: The Journal of Geology, v. 111, p. 505-523.

843 Searle, M., Parrish, R., Hodges, K., Hurford, A., Ayers, M., and Whitehouse, M., 1997, Shisha  
844 Pangma leucogranite, South Tibetan Himalaya: Field relations, geochemistry, age, origin,  
845 and emplacement: Journal of Geology, v. 105, p. 295-317.

846 Searle, M., Simpson, R., Law, R., Parrish, R., and Waters, D., 2003, The structural geometry,  
847 metamorphic and magmatic evolution of the Everest massif, High Himalaya of Nepal-  
848 South Tibet: Journal of the Geological Society, v. 160, p. 345-366.

849 Searle, M., Simpson, R., Law, R., Waters, D., and Parrish, R., 2002, Quantifying displacement  
850 on the South Tibetan Detachment normal fault, Everest massif, and the timing of crustal  
851 thickening and uplift in the Himalaya and Tibet: Journal of Nepal Geological Society, v.  
852 26, p. 1-6.

853 Searle, M. P., 1986, Structural evolution and sequence of thrusting in the High Himalayan,  
854 Tibetan-Tethys and Indus suture zones of Zaskar and Ladakh, western Himalaya:  
855 Journal of Structural Geology, v. 8, p. 923-936.

856 Searle, M. P., 1999, Extensional and compressional faults in the Everest-Lhotse Massif, Khumbu  
857 Himalaya, Nepal: Journal of the Geological Society, London, v. 156, p. 227-240.

858 Searle, M. P., Law, R. D., and Jessup, M. J., 2006, Crustal structure, restoration and evolution of  
859 the Greater Himalaya in Nepal--South Tibet: implications for channel flow and ductile  
860 extrusion of the middle crust, *in* Law, R., Searle, M., and Godin, L., eds., Channel Flow,  
861 Ductile Extrusion and Exhumation in Continental Collision Zones, Volume 268,  
862 Geological Society London Special Publication, p. 355-378.

863 Searle, M. P., and Rex, A. J., 1989, Thermal model for the Zaskar Himalaya: *Journal of*  
864 *Metamorphic Geology*, v. 7, p. 127-134.

865 Singh, S. K., Trivedi, J. R., and Krishnaswami, S., 1999, Re-Os isotope systematics in black  
866 shales from the Lesser Himalaya: Their chronology and role in the  $^{187}\text{Os}/^{188}\text{Os}$  evolution  
867 of seawater: *Geochimica et Cosmochimica Acta*, v. 63, p. 2381-2392.

868 Stöcklin, J., 1980, Geology of Nepal and its regional frame: *Journal of the Geological Society*,  
869 London, v. 137, p. 1-34.

870 Stüwe, K., and Foster, D., 2001,  $^{40}\text{Ar}/^{39}\text{Ar}$ , pressure, temperature and fission track constraints  
871 on the age and nature of metamorphism around the main central thrust in the eastern  
872 Bhutan Himalaya: *Journal of Asian Earth Sciences*, v. 19, p. 85-95.

873 Swapp, S. M., and Hollister, L. S., 1991, Inverted metamorphism within the Tibetan slab of  
874 Bhutan; evidence for a tectonically transported heat-source: *Canadian Mineralogist*, v.  
875 29, p. 1019-1041.

876 Tangri, S. K., and Pande, A. C., 1995, Tethyan Sequence, *in* Bhargava, O. N., ed., *The Bhutan*  
877 *Himalaya: a geological account*: Calcutta, Geological Survey of India, p. 109-141.

878 Tobgay, T., McQuarrie, N., Long, S., Kohn, M. J., and Corrie, S. L., 2012, The age and rate of  
879 displacement along the Main Central Thrust in the western Bhutan Himalaya: *Earth and*  
880 *Planetary Science Letters*, v. 319-320, p. 146-158.



881 Valdiya, K. S., 1980, Geology of the Kumaun Lesser Himalaya, Dehra Dun, Wadia Institute of  
882 Himalayan Geology.

883 Valdiya, K. S., 1989, Trans-Himadri intracrustal fault and basement upwarps south of the Indus-  
884 Tsangpo suture zone, *in* Malinconico, L., and Lillie, R., eds., Tectonics of the western  
885 Himalayas, Volume 232, Geological Society of America Special Paper, p. 153-168.

886 Vannay, J.-C., and Hodges, K., 1996, Tectonometamorphic evolution of the Himalayan  
887 metamorphic core between the Annapurna and Dhaulagiri, central Nepal: *Journal of*  
888 *Metamorphic Geology*, v. 14, p. 635-656.

889 Walker, J. D., Martin, M. W., Bowring, S. A., Searle, M. P., Waters, D. J., and Hodges, K. V.,  
890 1999, Metamorphism, melting, and extension: age constraints from the High Himalayan  
891 slab of southeast Zaskar and northwest Lahaul: *Journal of Geology*, v. 107, p. 473-495.

892 Wang, Z., and Zhen, X., 1975, Imbricate structure in the northern slope of Jolmo Lungma and  
893 discussion of the uplift of the Himalaya, *Scientific exploration of Jolmo Lungma:*  
894 *Beijing, Science Publishing House*, p. 199-221.

895 Wopenka, B., and Pasteris, J. D., 1993, Structural characterization of kerogens to granulite facies  
896 graphite; applicability of Raman microprobe spectroscopy: *American Mineralogist*, v. 78,  
897 p. 533-557.

898 Wu, C., Nelson, K. D., Wortman, G., Samson, S. D., Yue, Y., Li, J., Kidd, W. S. F., and  
899 Edwards, M. A., 1998, Yadong cross structure and South Tibetan Detachment in the east  
900 central Himalaya (89-90°E): *Tectonics*, v. 17, no. 1, p. 28-45.

901 Yin, A., 2006, Cenozoic tectonic evolution of the Himalayan orogen as constrained by along-  
902 strike variation of structural geometry, exhumation history, and foreland sedimentation:  
903 *Earth Science Reviews*, v. 76, p. 1-131.

904 Yin, A., Dubey, C. S., Kelty, T. K., Webb, A. A. G., Harrison, T. M., Chou, C. Y., and Celerier,  
905 J., 2010, Geologic correlation of the Himalayan orogen and Indian craton: Part 2.  
906 Structural geology, geochronology, and tectonic evolution of the Eastern Himalaya:  
907 Geological Society of America Bulletin, v. 122, no. 3/4, p. 360-395.

908 Yin, A., Harrison, T. M., Ryerson, F. J., Chen, W., Kidd, W. S. F., and Copeland, P., 1994,  
909 Tertiary structural evolution of the Gangdese thrust system, southeastern Tibet: Journal of  
910 Geophysical Research, v. 99, p. 18175-18201.

911

## 912 **FIGURE CAPTIONS**

913 **Figure 1.** Simplified geologic map of Bhutan and surrounding regions. Compiled from Gansser  
914 (1983), Bhargava (1995), Grujic et al. (2002), Long and McQuarrie (2010), Long et al. (2011c),  
915 Hughes et al. (2011), and Cooper et al. (in press). Box indicates the location of the study area  
916 shown in Figure 3. Inset map: A simplified tectonic map of the Himalayan orogen (modified  
917 from Hodges (2000) and Long et al. (2011c)). Abbreviations: STFS = South Tibetan fault  
918 system; KT = Kakhtang thrust; MCTS = Main Central thrust system; MBTS = Main Boundary  
919 thrust system; MFTS = Main Frontal thrust system; PW = Paro window; YCS = Yadong cross  
920 structure; Jo = Mount Jomolhari; KK = Khula Kangri pluton; WL = Wagye La; GL = Gonto La;  
921 LLK = Lhozhag La Kang; DCK = Dang Chu (Tang Chu) klippe; UK = Ura klippe; ZK =  
922 Zhemgang (Black Mountain) klippe; SK = Sakteng (Radi) klippe. Interpreted contacts at the base  
923 of the Dang Chu, Ura, and Zhemgang klippen follow Long and McQuarrie (2010). Cross-section  
924 line A–A' refers to Figures 3 and 9.

925

926 **Figure 2.** Alternative geologic interpretations of central Bhutan. (a) Long and McQuarrie (2010)  
927 interpret the Dang Chu and Ura klippen as being soled by the STFS but map the GHS-Chekha  
928 contact at the base of the Zhemgang klippe as a conformable contact. The breakaway zone for  
929 the STFS is inferred to lie between the two klippen. (b) Grujic et al. (2011) map the Chekha  
930 Formation more extensively across central Bhutan, joining the Dang Chu and Zhemgang klippen  
931 and extending the Ura klippe northward, where it is cut by the Kakhtang Thrust. RSCM  
932 sampling locations for this study and the location of Cambrian fossils found by Hughes et al.  
933 (2011) are shown. The RSCM results are split into three groups according to peak metamorphic  
934 temperature. Abbreviations follow Figure 1. Stars refer to outcrop photographs in Figure 4.

935  
936 **Figure 3.** Schematic cross-sections for the contrasting geological interpretations of (a) Long and  
937 McQuarrie (2010) and (b) Grujic et al. (2011). In (a), the distance between the STFS breakaway  
938 zone and the Ura klippe to the north implies a maximum displacement on the STFS of ca. 20 km.  
939 In (b), the distance from the STFS exposed at the crest of the range to the southernmost extent of  
940 the Zhemgang klippe implies a minimum displacement of 100 km on the STFS.

941  
942 **Figure 4.** Outcrops of Tibetan Sedimentary sequence, Chekha Formation, and Greater  
943 Himalayan sequence units illustrating differences in structural style. Locations are shown in  
944 Figure 2. (a) and (b) Large-scale recumbent folding in TSS marbles of the Dang Chu klippe, (a)  
945 next to the Baylangdra monastery, and (b) at Pele La. (c) A cliff of Chekha Formation quartzite  
946 in the Dang Chu klippe dips consistently to the north and shows no evidence for large scale  
947 folding. This fundamental change in structural style is the same as the change across the STFS  
948 mapped by Cooper et al. (in press) in the Jomolhari area of NW Bhutan. (d) GHS pelitic schists

949 north of the Ura klippe show a similar consistently north-dipping fabric, with no large-scale  
950 folding. (e) Chekha Formation quartzites and (f) interbedded quartzite and phyllite of the TSS  
951 Maneting formation (as mapped by Long et al. (2011c) in the Zhemgang klippe dips gently to the  
952 south and also shows no evidence for large-scale folding.

953

954 **Figure 5.** Simplified stratigraphic columns for central Bhutan showing how different research  
955 groups have interpreted the stratigraphy and positions of the major fault systems. For  
956 abbreviations, see Figure 1. Age ranges follow Hughes et al. (2011); Long and McQuarrie  
957 (2010); and Tangri and Pande (1995). Unit thicknesses (shown in kilometers on the right hand  
958 side of each column) are from Long and McQuarrie (2010); Long et al. (2011a); and Tangri and  
959 Pande (1995).

960

961 **Figure 6.** Examples of Raman spectra for each sample. The positions of the graphite band, G,  
962 and defect bands D1 and D2 are indicated. R2 values and temperatures calculated using the  
963 Beyssac et al. (2002a) calibration are given. Full details of peak positions for individual analyses  
964 are given in Data Repository Item B.

965

966 **Figure 7.** All 17 samples plotted in order of peak metamorphic temperature. 13 samples (FB52  
967 to FB102) show very consistent temperatures, with an error-weighted mean average of  $560 \pm$   
968  $2^{\circ}\text{C}$  (2SE). These samples include TSS marbles and phyllites (Maneting Formation), Chekha  
969 Formation schists, quartzites, and calc-silicates as well as GHS paragneisses and schists across  
970 all three klippen (Figure 2). The lack of any temperature difference between the Chekha, GHS,  
971 and TSS Maneting Formation samples suggests that there is no metamorphic discontinuity across

972 between them. Four samples give distinctly lower temperatures: Samples FB64 and FB85, both  
973 foliated calc-silicates, give temperatures of  $508 \pm 33^\circ\text{C}$  and  $489 \pm 26^\circ\text{C}$  (2SE), respectively,  
974 while samples FB28, a marble and FB77, a black shale give  $430 \pm 30^\circ\text{C}$  and  $420 \pm 21^\circ\text{C}$ ,  
975 respectively.

976

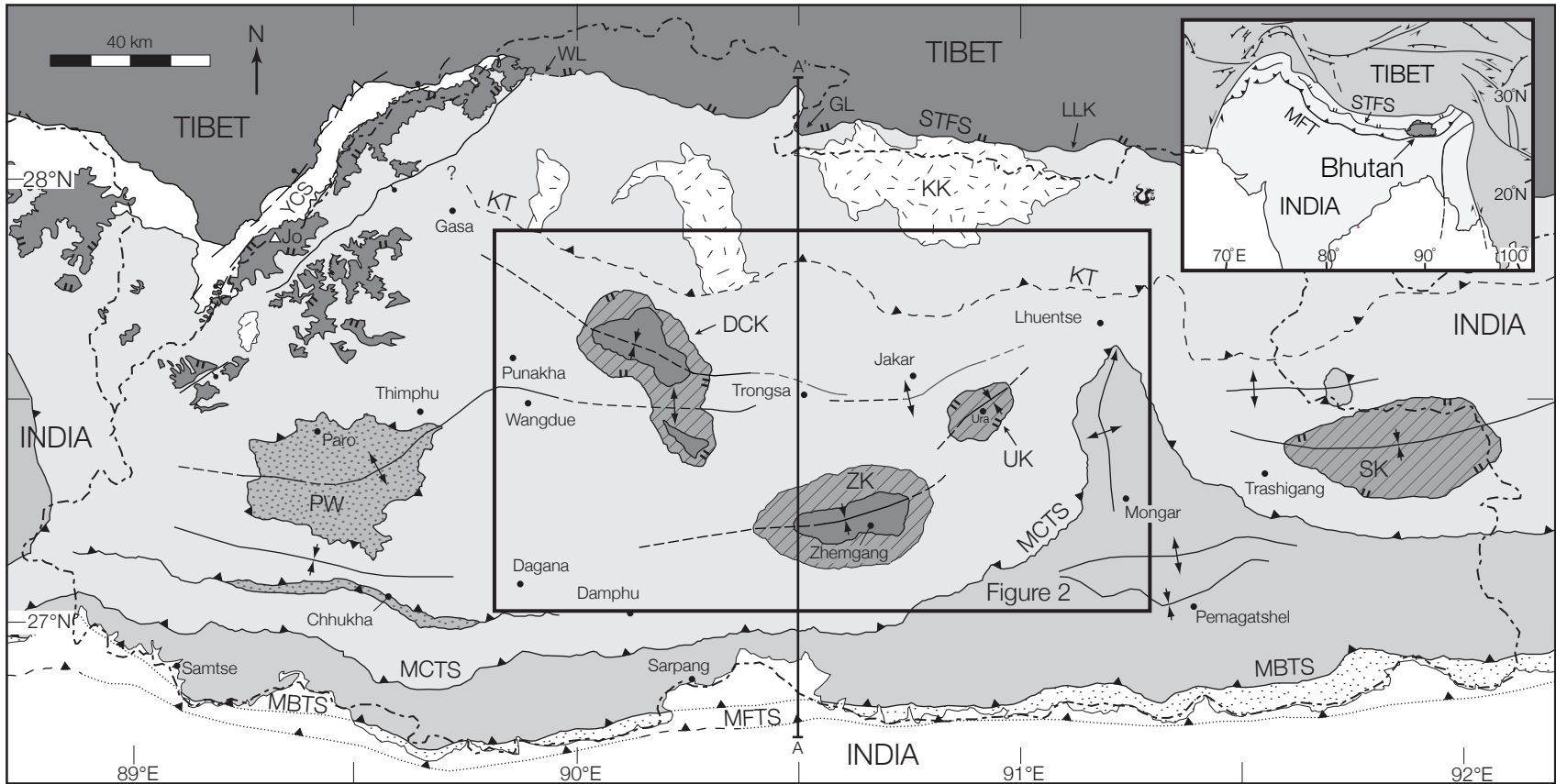
977 **Figure 8.** Our interpretation for the distribution of RSCM temperatures in central Bhutan.  
978 Abbreviations: DCKn = Dang Chu klippe, north; DCKs = Dang Chu klippe, south; STFS =  
979 South Tibetan fault system; KT = Kakhtang thrust; MCTS = Main Central thrust system; MBTS  
980 = Main Boundary thrust system. (a) The Chekha Formation and GHS are combined as one  
981 sequence due to their similar lithology, structural style and peak metamorphic temperature. The  
982 TSS in the Dang Chu klippe is mapped on the basis of the four lower-temperature samples,  
983 FB28, FB64, FB77 and FB85 as well as our structural observations of recumbently folded units  
984 and the location of fossils found by Hughes et al. (2011). We interpret the contact between the  
985 TSS and structurally lower units to be the sole STFS detachment. (b) Schematic cross-section  
986 through the north and south components of the Dang Chu klippe. The distance from the STFS  
987 exposed at the crest of the range to the southernmost extent of the Dang Chu klippe implies a  
988 minimum displacement of 80 km on the STFS.




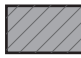



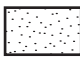


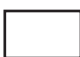
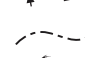


989

990

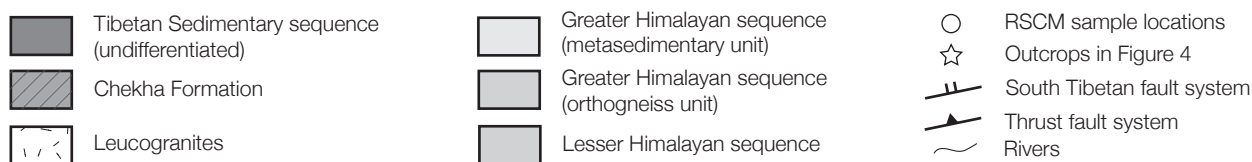
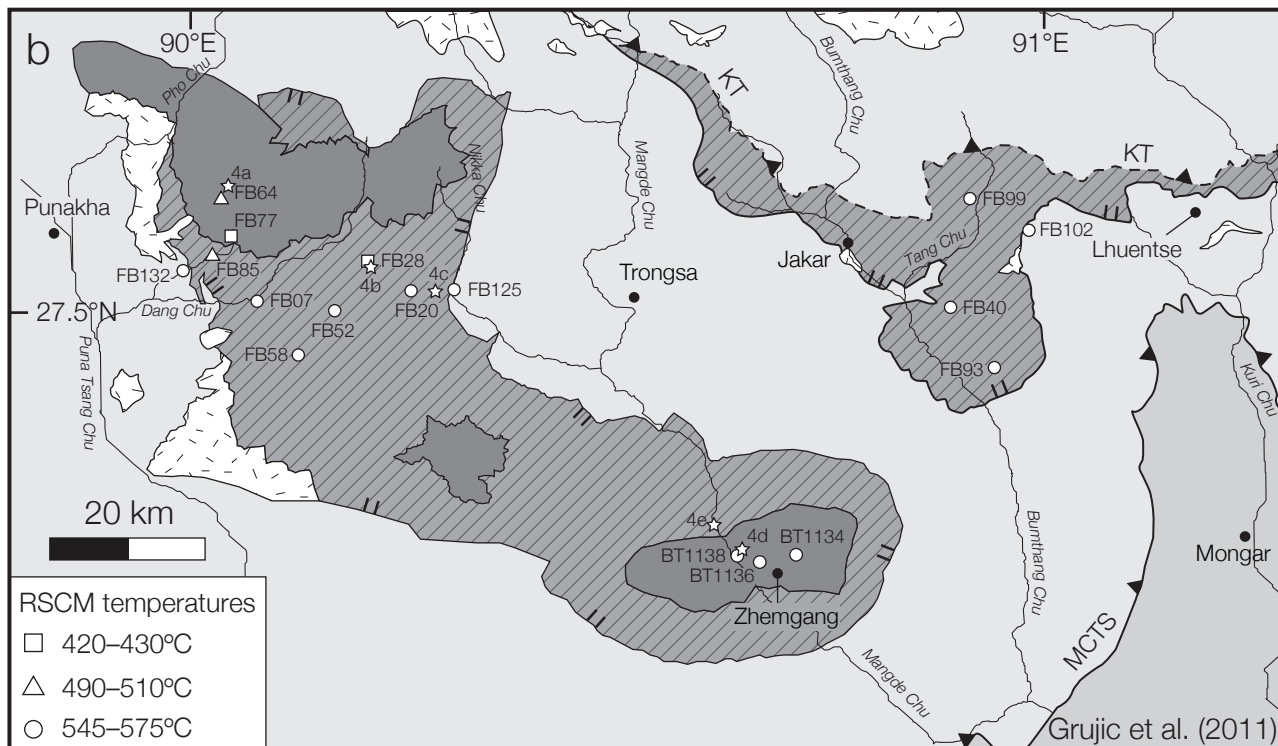
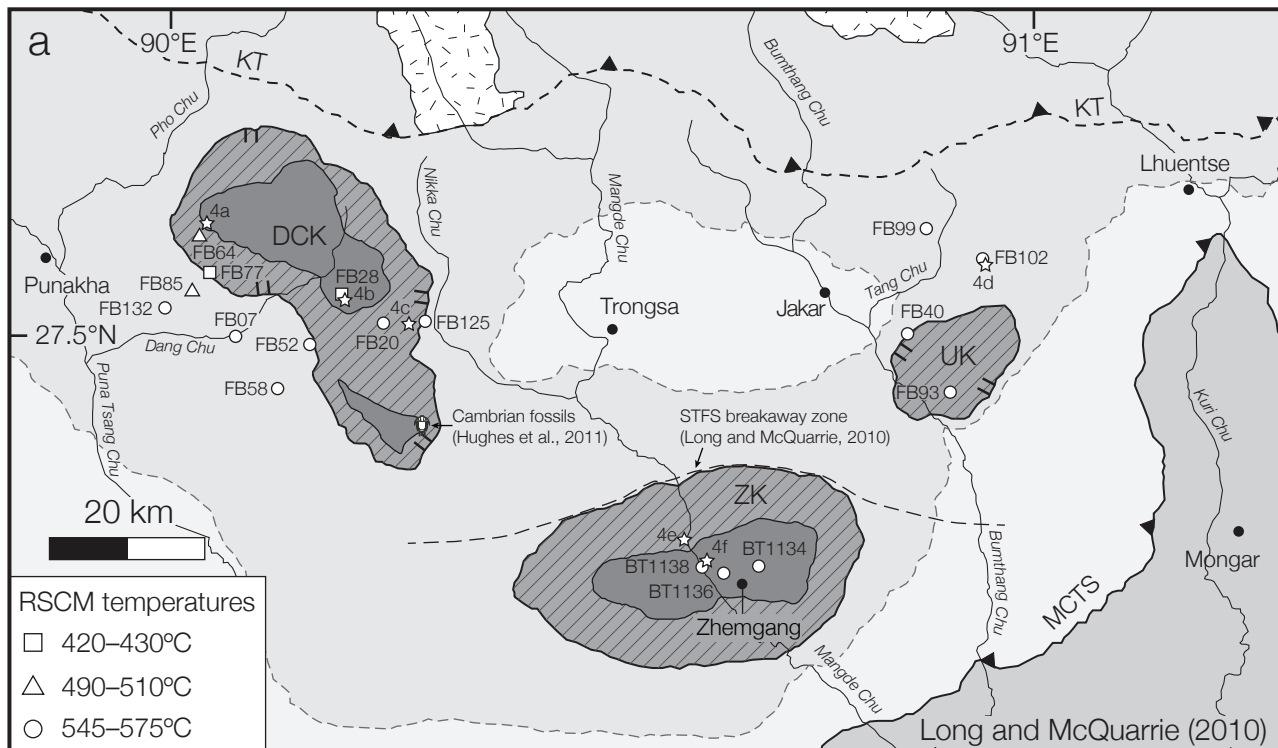
991 <sup>1</sup>GSA Data Repository item 2012xxx, Examples of analyzed carbonaceous material, complete  
992 RSCM spectra data, and thermobarometric methods and data tables, is available online at  
993 [www.geosociety.org/pubs/ft2009.htm](http://www.geosociety.org/pubs/ft2009.htm), or on request from [editing@geosociety.org](mailto:editing@geosociety.org) or Documents  
994 Secretary, GSA, P.O. Box 9140, Boulder, CO 80301, USA.

Cooper et al. Figure 1

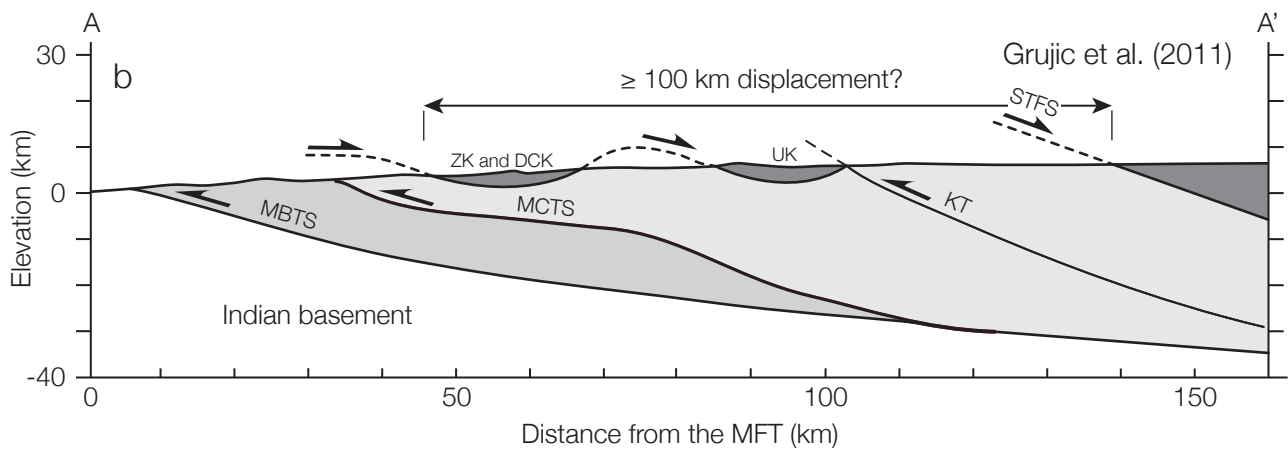
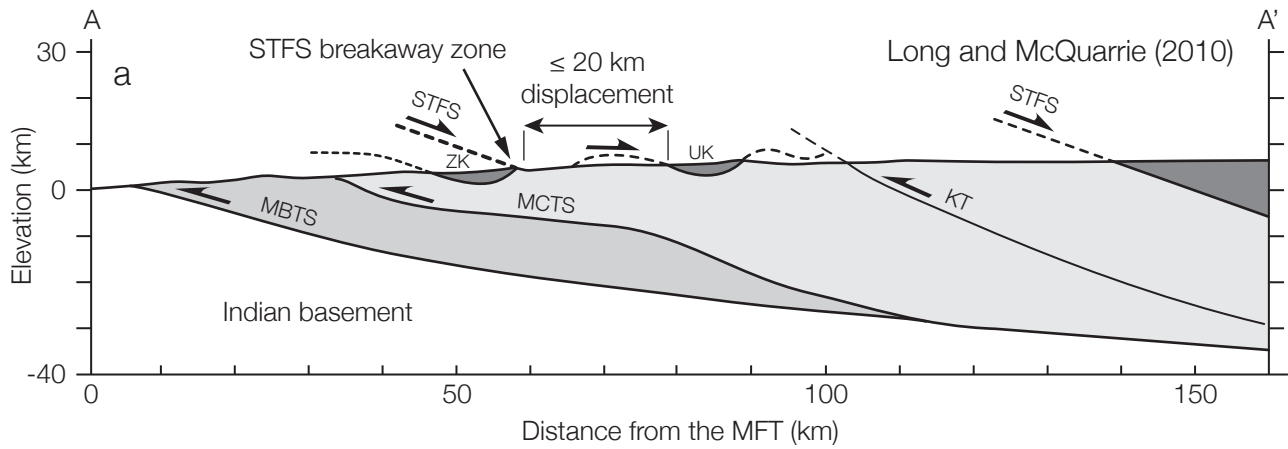


- |   |   |   |  |   |                                   |
|---|---|---|--|---|-----------------------------------|
|  | Tibetan Sedimentary sequence (TSS) (undifferentiated) |  | Paro Formation                                     |  | South Tibetan fault system (STFS) |
|  | Chekha Formation                                      |  | Lesser Himalayan sequence (LHS) (undifferentiated) |  | Thrust fault system               |
|  | Leucogranites   |  | Subhimalaya (Siwalik Group)                        |  | High-angle normal fault           |
|  | Greater Himalayan sequence (GHS) (undifferentiated)   |  | Quaternary sediment                                |  | Syncline; anticline               |
|   |   |   |  |  | International border              |
|   |   |   |  |  | Dragons                           |

Cooper et al. Figure 2

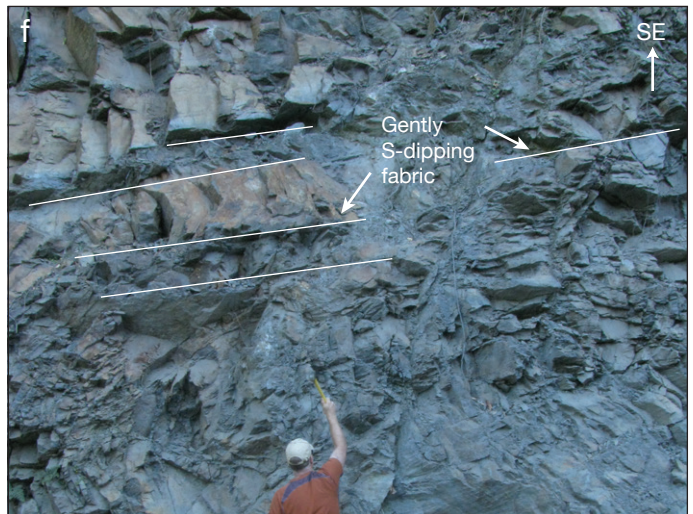
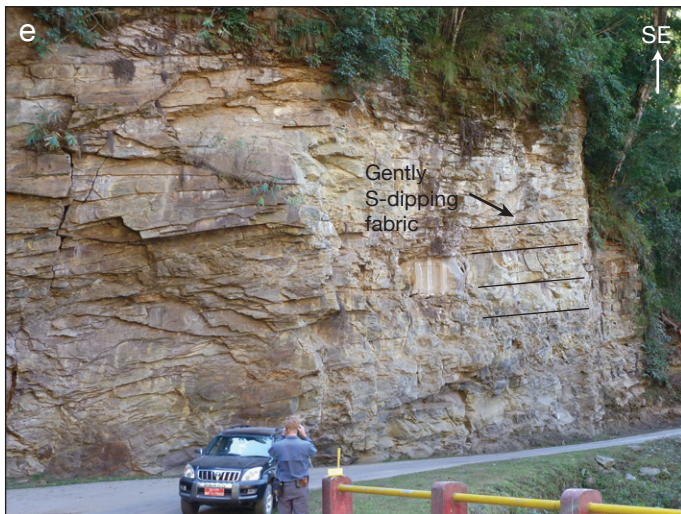
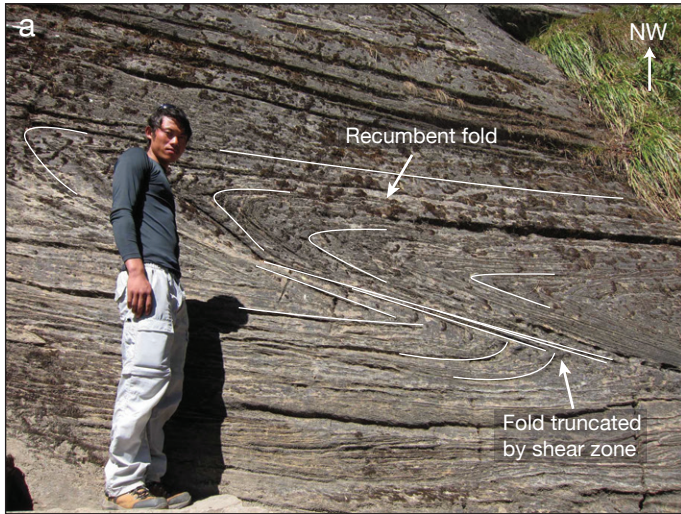


Cooper et al. Figure 3





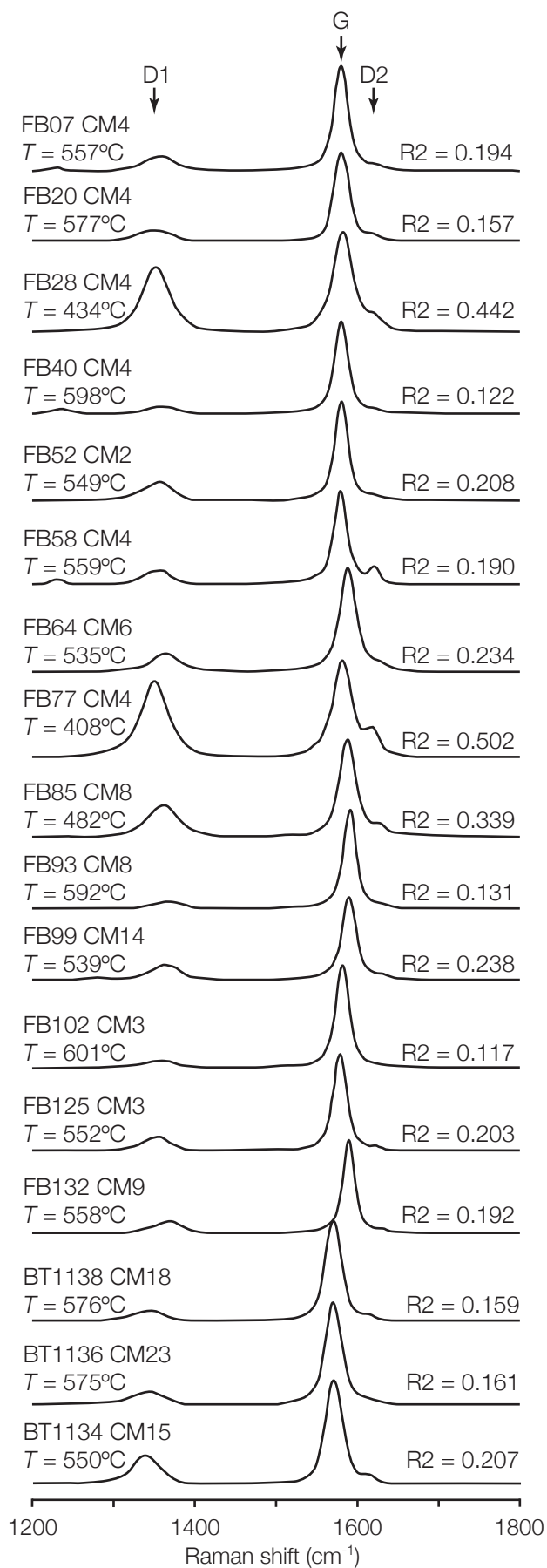
Cooper et al. Figure 4



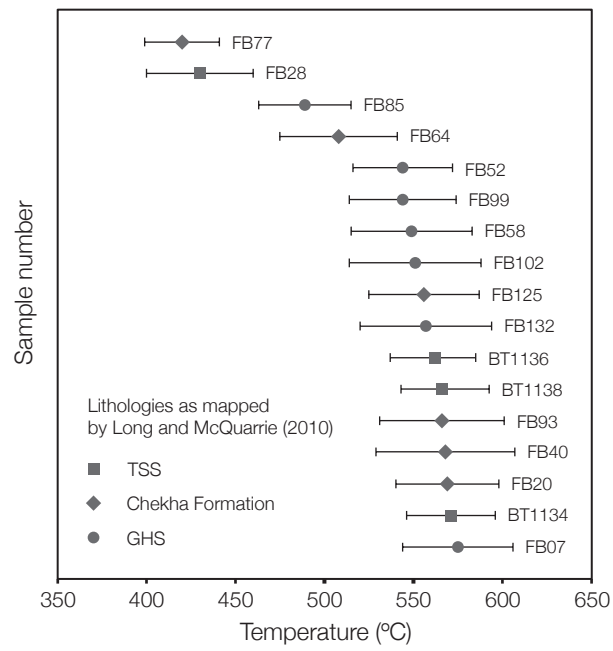
Cooper et al. Figure 5

Long and McQuarrie (2010)			Grujic et al. (2011)			This study		
TSS	Undifferentiated units (Paleozoic-Mesozoic[?])	>1.0	TSS	Undifferentiated units (Paleozoic-Mesozoic[?])	>1.0	TSS	Tang Chu and Pele La Groups, undifferentiated (Paleozoic-Mesozoic[?]) $\swarrow$ STFS	>0.9
	Maneting Fm. (Cambrian[?])	>1.0		TSS	Chekha Formation (Neoproterozoic-Ordovician[?]) depositional or $\swarrow$ STFS	2.2-4.0	GHS	Chekha and Maneting Formations, undifferentiated (Neoproterozoic-Ordovician[?])
GHS	GHS metasedimentary unit (Neoproterozoic-Ordovician[?])	0.5-6.7	GHS		GHS orthogneiss unit (Cambrian-Ordovician) $\swarrow$ STFS	2.7-10.7		GHS
	GHS orthogneiss unit (Cambrian-Ordovician) $\swarrow$ MCTS	1.5-8.0		GHS	GHS orthogneiss unit (Cambrian-Ordovician) $\swarrow$ MCTS	1.5-8.0	GHS	

Cooper et al. Figure 6



Cooper et al. Figure 7



Cooper et al. Figure 8

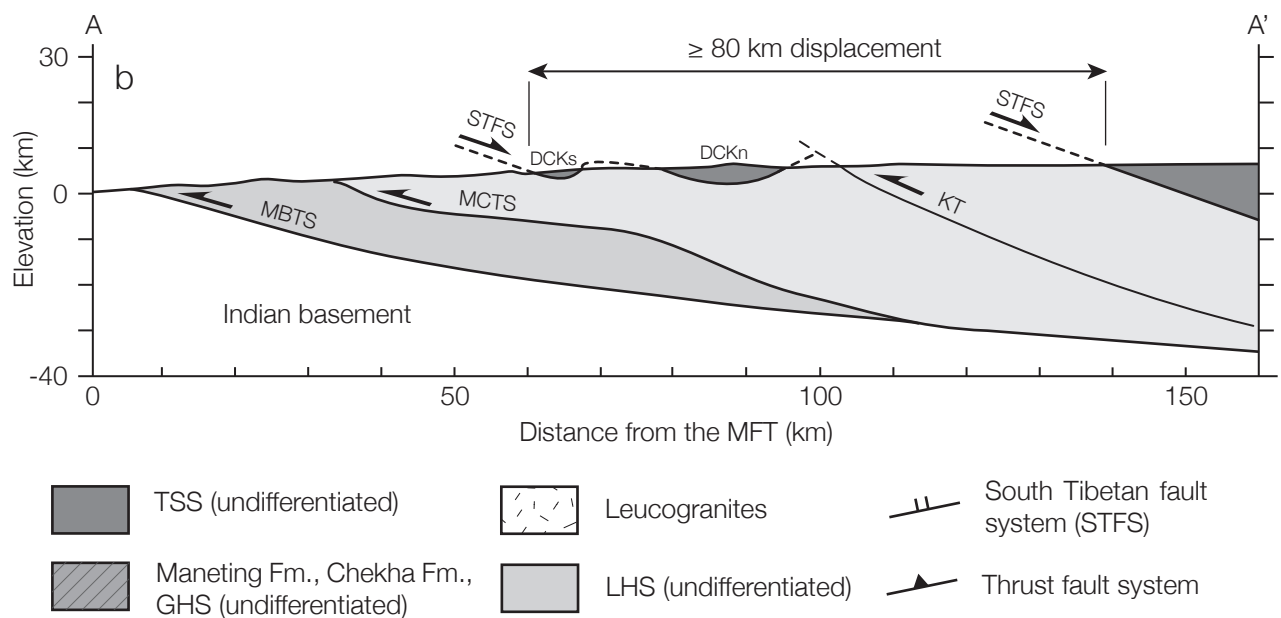
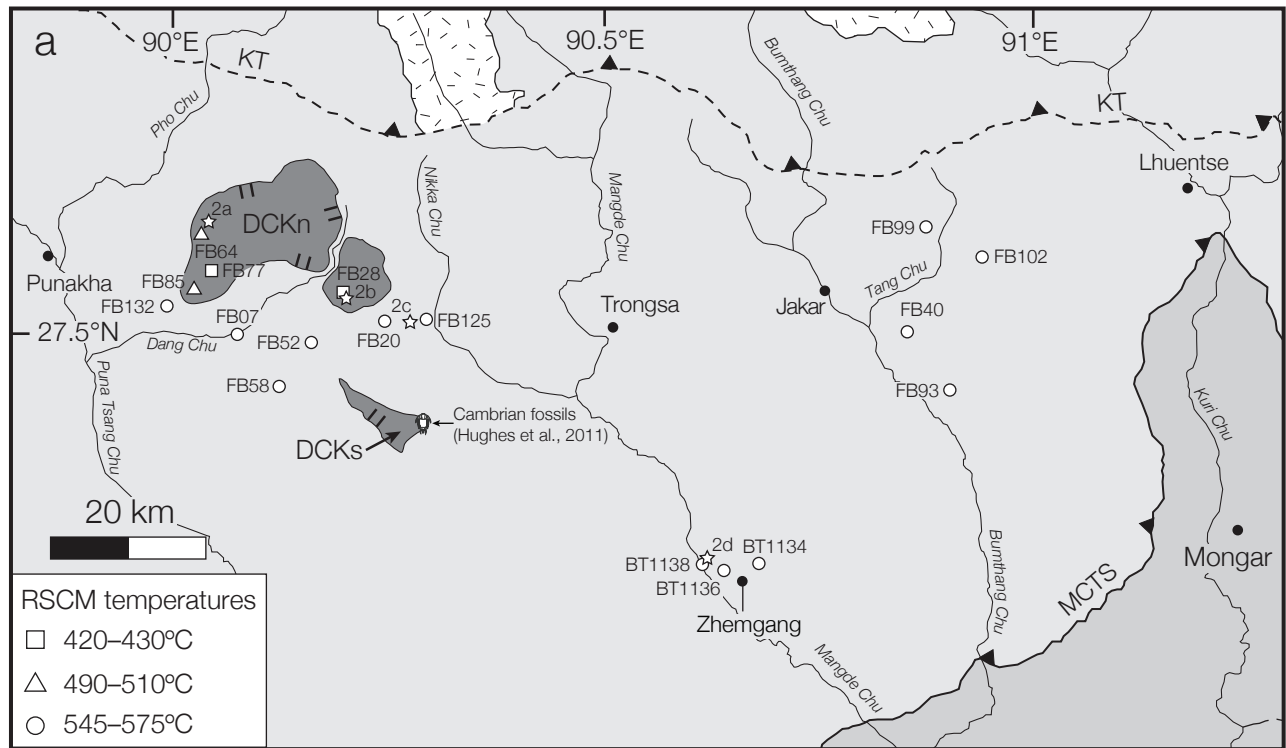


Table 1. RSCM temperatures

Sample	Lithology	Location		R2		Temp (°C)			n
		Latitude (°)	Longitude (°)	Mean	1 $\sigma$	Mean	1 $\sigma$	2SE	
FB07	Paragneiss	27.505	90.078	0.165	0.090	575	49	31	20
FB20	Quartzite	27.518	90.250	0.175	0.071	569	40	29	20
FB28	Marble	27.551	90.202	0.454	0.073	430	31	30	15
FB40	Paragneiss	27.504	90.854	0.178	0.104	568	57	39	15
FB52	Pelitic schist	27.496	90.165	0.220	0.073	544	39	28	20
FB58	Quartzite	27.445	90.127	0.212	0.080	549	43	34	15
FB64	Calc-silicate	27.617	90.036	0.288	0.082	508	40	33	15
FB77	Graphitic slate	27.577	90.048	0.474	0.038	420	16	21	25
FB85	Calc-silicate	27.556	90.028	0.326	0.061	489	31	26	20
FB93	Pelitic schist	27.436	90.905	0.169	0.105	566	47	35	15
FB99	Marble	27.625	90.876	0.220	0.083	544	46	30	20
FB102	Paragneiss	27.591	90.941	0.209	0.098	551	52	37	15
FB125	Paragneiss	27.520	90.299	0.200	0.098	556	53	31	22
FB132	Paragneiss	27.537	89.997	0.200	0.122	557	66	37	20
BT1134	Phyllite	27.236	90.681	0.171	0.070	571	39	25	25
BT1136	Phyllite	27.228	90.638	0.189	0.060	561	33	24	25
BT1138	Phyllite	27.234	90.615	0.179	0.055	566	31	23	25

R2 values calculated using the calibration of Beyssac et al. (2002a) and temperatures calculated using Aoya (2010). Variability of the R2 value within each sample is indicated by its 1 $\sigma$  uncertainty.

Temperatures are reported as standard means at the 1 $\sigma$  and 2 standard errors (2SE) confidence levels, accounting for both internal and external uncertainties (see also Data Repository Item B).

Table 2. RSCM vs GARB-GMBP results

Sample	RSCM <sup>a</sup>			GARB <sup>b</sup>		GMBP <sup>b</sup>		
	Temp (°C)		n	Temp (°C)		Pressure (kbar)		n
	Mean	2SE		Mean	2SE	Mean	2SE	
FB07	575	31	20	579	48	5.0	0.6	3
FB125	556	31	22	532	56	6.2	0.8	4
FB132	557	37	20	536	75	4.5	0.8	3

<sup>a</sup>RSCM temperatures were calculated using the Aoya (2010) calibration.

<sup>b</sup>GARB temperatures and GMBP pressures were calculated using THERMOCALC v. 3.33. All data are reported as means at the 2 standard errors confidence level.